12-13-2002

Upgrading and Qualification of a Turbulent Heat Transfer Test Facility

Olumide Folorunso Odetola

UPGRADING AND QUALIFICATION OF A TURBULENT HEAT TRANSFER TEST FACILITY

By

Olumide Folorunso Odetola

A Thesis
Submitted to the Faculty of
Mississippi State University
in Partial Fulfillment of the Requirements
for the Degree of Master of Science
in Mechanical Engineering
in the Department of Mechanical Engineering

Mississippi State, Mississippi

December 2002

UPGRADING AND QUALIFICATION OF A TURBULENT HEAT TRANSFER TEST FACILITY

By

Olumide Folorunso Odetola

Approved:

James A. Parsons Assistant Professor of Mechanical Engineering (Major Professor)	Rogelio Luck Associate Professor of Mechanical Engineering Graduate Coordinator of the Department of Mechanical Engineering
B. Keith Hodge Professor of Mechanical Engineering (Committee Member)	Robert P. Taylor Professor of Mechanical Engineering and Associate Dean of the College of Engineering (Committee Member)
W. Glenn Steele Professor and Departmental Head of Mechanical Engineering	A. Wayne Bennett Dean of the College of Engineering

Name: Olumide Folorunso Odetola

Date of Degree: December 13, 2002

Institution: Mississippi State University

Major Field: Mechanical Engineering

Major Professor: Dr. James A. Parsons

Title of Study: UPGRADING AND QUALIFICATION OF A TURBULENT HEAT TRANSFER TEST FACILITY

Pages in Study: 83

Candidate for Degree of Master of Science

The Turbulent Heat Transfer Test Facility (THTTF) has been refurbished and the data acquisition system upgraded. The THTTF is now controlled by a LabView 4.1 program which replaces the old program in BASIC. Heat transfer data acquired using this new program is presented as Stanton number distributions. The new data set is compared to previously reported data obtained with this facility and other well-accepted published data. This project has successfully qualified the THTTF for zero-pressure gradient, isothermal wall temperature, incompressible boundary-layer flow over smooth flat plates without transpiration.

The THTTF is now set to accommodate modifications which will facilitate heat transfer investigations with high freestream turbulence.

DEDICATION

This research is dedicated to the memory of my father, Dr. Adebayo Odetola, and to my mother Dr. Adebimpe Odetola, my wife and son, Oluwatosin and Boluwatife, for their love, encouragement and guidance and for believing in me.

ACKNOWLEDGEMENTS

I would like to express my sincere gratitude to the members of my committee for their guidance and assistance without which this thesis could not have been completed. First, Dr James Parsons, my major professor for his patience and willingness to teach. Sincere thanks also go to Dr. B. Keith Hodge and Dr. Robert P Taylor for serving on my committee and for their invaluable advice and consultation. Expressed appreciation is also due to Dr. W. Glenn Steele, Dr. George Adebiyi (and family), and Dr. William Person for providing the required support and encouragement.

My heartfelt appreciation also goes to my family, my beloved wife, Oluwatosin, and our son, Boluwatife, for their understanding, patience and endurance during this period.

Above all, I thank the Almighty God for His loving kindness and Grace through Jesus Christ, which sustained me through this program and gives hope for a blessed tomorrow.

TABLE OF CONTENTS

LIST OF TABLES

LIST OF FIGURES

NOMENCLATURE

A	Plate surface area
B	Bias limit
C_P	Specific heat of the freestream air
C_f	Skin friction coefficient
h	Convective heat transfer coefficient
r	Recovery factor
R	Resistance
Re_x	x-Reynolds number
$Re_{\Delta 2}$	Enthalpy thickness Reynolds number
P	Pressure
Pr	Prandtl number
Q_c	Conductive heat loss rate
Q_r	Radiative heat loss rate
St	Stanton number
T_r	Recovery temperature
T_o	Total temperature
T_p	Plate surface temperature
T_∞	Freestream static temperature
Tu	Turbulence intensity

U_∞	Freestream velocity
$(UA)_{eff}$	Effective conductance
V	Voltage

Greek

ε	Plate surface emissivity
ν	Kinematic viscosity
μ	Dynamic viscosity
ρ	Density
σ	Stephan-Boltzmann constant
Δ	Boundary layer integral thickness
Δ_2	Enthalpy thickness
θ	Momentum thickness
Λ_x	Integral length scale
Lu^{ε}	Dissipation length scale

CHAPTER I

INTRODUCTION

Most engineering fluid flow applications operate in the turbulent flow regime with aerodynamically rough surfaces. Accurate aerodynamic and heat transfer predictions are thus required in the design of such applications as gas turbine blades, combustors, heat exchangers, re-entry vehicles, aircraft skin, and piping systems. It has also been determined that heat transfer and skin friction can be significantly higher for flows over rough surfaces as compared with equivalent flows over smooth surfaces.

High freestream turbulence levels have significant effects on the heat transfer and skin friction characteristics. Although much of the work done so far in investigating the effects of turbulence have been done with low freestream turbulence levels in the order of 3 to 5%, Koutomos and McGuirk (1989) measured typical freestream turbulence levels in gas turbines and reported levels greater than 20%.

Background Work On Roughness

The current trend in gas turbine design is to improve efficiency by operating at higher, more efficient temperatures. With advances in materials and component cooling technologies, progressively higher operating temperatures have been achieved, thus reducing fuel consumption without compromising component integrity due to the large induced thermal and mechanical stresses. Therefore, there is an increasing need for models to accurately predict the heat and fluid characteristics of turbulent freestream flow over such rough surfaces.

The effect of surface roughness on heat transfer and fluid dynamics has been a subject of interest for many engineers. Early efforts by Nikuradse (1933), Schlichting (1936), and Moody (1944) provide the fundamental data for turbulent flow analysis. Background work by Nikuradse provided pressure drop and velocity measurements in pipes roughened with sand grains and generated results for a range of grain sizes. The equivalent sand-grain roughness is defined as the sand-grain size in Nikuradse's experiment that gives the same flow resistance at the same flow Reynolds number. Flow resistance data must be available to determine the equivalent sand grain roughness. Equivalent sand grain modeling involves measuring skin friction and velocity profiles for a rough surface and comparing the results with data from Nikuradse's experiment.

Moody's work provides the first universally accepted method for friction prediction and is presented as the well-known Moody diagram. Attempts to develop correlations for heat transfer based on the equivalent sand grain roughness concept have recorded limited success. This is because the sand grain concept is basically momentum-transport based and is not easily adapted accurately to heat transfer which is basically energy-transport based. The best known correlation is that of Seidman (1978) which assumes a unique correlation between the heat transfer and the skin friction. However, in many cases this assumption is not valid.

Over the past two decades, a predictive approach that does not depend on the equivalent sandgrain concept has been developed. This approach is known as the discrete-element model and is based on the idea that skin friction and heat transfer characteristics are composed of two distinct contributions:

1. that due to the roughness elements
2. that due to the smooth surface between the roughness elements

In the discrete element approach, the effects of the roughness elements on momentum and energy transfer are incorporated into the governing equations. Three major effects of the roughness elements on the flow field are identified below:

1. Blockage in flow caused by the decrease in flow area due to the space occupied by the roughness elements.
2. Form drag which results as the fluid flows over and around an element.
3. Local heat transfer between the element and the fluid if the element surface is at a different temperature from the fluid.

Previous Efforts With The THTTF

Numerous studies have been done to determine the effects of surface roughness on heat transfer and skin friction. However, most of the roughness-influenced turbulence data available have been on ill-defined rough surfaces, with the reported results having equivalent sand-grain roughness values implicitly included at some stage of the data reduction.

A reevaluation of Schlichtings data by Coleman, Hodge, and Taylor (1984) found that Schlichting had made erroneous assumptions in his data reduction, which significantly affected the reported data. Thus, the previous data sets suffered from inherent inaccuracies. The Turbulent Heat Transfer Test Facility (THTTF) was designed to investigate and provide highly-accurate data on the heat transfer and fluid dynamic characteristics of turbulent flow over rough surfaces.

Coleman et al. (1988) successfully completed the smooth-wall qualification of the THTTF and reported skin friction and Stanton number data on an aerodynamically smooth surface. They compared heat transfer data with the data of Reynolds, Kays and Kline (1958) and the correlation of Moffat (1967). The qualification checks showed an experimental Stanton number uncertainty of 2-5% depending on the flow conditions.

Following this qualification check, Hosni et al. (1989) investigated the effects of roughness for zero-pressure gradient turbulent boundary layers. This experiment compared results for an aerodynamically-smooth surface with three well-defined rough surfaces for freestream velocities ranging from 6m/s to 67 m/s. The rough surfaces were composed of 1.27 mm diameter hemispheres spaced 2, 4, and 10 diameters apart in, staggered arrays. The results of Hosni et al (1989) show an increase in skin friction and Stanton number as the surface roughness increases.

From 1988 to 1992 Taylor and others performed various experiments to determine the effects of different thermal boundary conditions on the heat transfer for different levels of surface roughness. Boundary conditions investigated include constant wall temperature, constant wall heat flux, step wall temperature, and piecewise linear wall temperature distribution. During this period, the THTTF was also used to investigate the effects of pressure gradient on flow and heat transfer using different rough surfaces. Details for these MSU experiments can be obtained from the list of references at the end of this report.

Details of the uncertainty analysis in the experimental Stanton number determination for this apparatus are presented in Appendix A.

Previous High Freestream Turbulence Studies

There have been several studies attempting to determine the effects of freestream turbulence on skin friction and heat transfer. Turbulence intensity is defined as the ratio of the fluctuating streamwise rms velocity to the mean freestream velocity. Two turbulent length scales often used are the integral length scale, Λ_x, and the dissipation length scale, Lu^{ε}. Details of the definition and derivation of these length scales are presented in Thole (1992).

The enhancements in shear stress and heat transfer due to freestream turbulence are normally measured as a skin friction coefficient ratio and a Stanton number ratio, respectively. The skin friction coefficient ratio is defined as C_f / C_{fo}, where C_{fo} is the shear stress for a standard (low freestream turbulence) boundary layer at the same momentum thickness Reynolds number, Re_θ. The Stanton number ratio is likewise defined as St / St_o, where St_o is the Stanton number for a standard boundary layer at the same Re_θ or enthalpy thickness Reynolds number, $Re_{\Delta 2}$.

Most of the data in the published literature are for grid-generated freestream turbulence. Grid-generated turbulence has been reported to be limited to about 7-10%, except for immediately downstream the grid but the flow profile at this location is highly non-uniform. Several correlations have been proposed based on these studies done with relatively low turbulence levels. One of the earliest reported studies is that of Kestin (1966) who investigated the influence of turbulence on heat transfer from plates with and without pressure gradient.

Simonich and Bradshaw (1978) used grids of different sizes to generate turbulence levels up to 7% and found that for a 1% increase in longitudinal turbulence at constant Re_θ, the ratio C_f / C_{fo} increased by 2% while St/St_o increased by 5%.

The most widely used correlation is provided by Hancock and Bradshaw (1983) who investigated the effects of length scale and freestream turbulence levels on the velocity boundary layer. They correlated the skin friction ratio with a parameter β, based on both the turbulence level and length scale.

$$\beta = \frac{Tu \quad (\%)}{\frac{L_u^{\varepsilon}}{\delta} + 2} \tag{1.1}$$

This parameter implies that as the length scale is increased for a given turbulence level, β will decrease and hence the expected shear stress enhancement will decrease.

Blair (1983) studied the effects of freestream turbulence on skin friction and heat transfer in the range $0.25 < \beta < 1$ and length scale ratio $0.2 < Lu^{\varepsilon}/\delta_{99} < 2$. He found that at low Re_{θ}, the skin-friction enhancement due to freestream turbulence was suppressed. Blair also found that the heat-transfer enhancement due to increasing levels of freestream turbulence were higher than the corresponding increase in skin friction.

Castro (1984) investigated the effects of freestream turbulence on low Reynolds number velocity boundary layers and found that the effects of Reynolds number became increasingly less significant as the freestream turbulence levels increased.

Some experimental studies with high freestream turbulence levels (greater than 7%) have recently been conducted. These efforts have extended the range of the β parameter proposed by Hancock and Bradshaw (1983) and provided new alternative correlating parameters. MacMullin, Elrod, and River (1989) used a wall jet to generate turbulence levels as high as 20%. The flow field for this experiment was characteristically different, having a highly non-uniform streamwise mean velocity profile. MacMullin et al. found a large scatter when the St/St_o ratio data were plotted in terms of the β parameter at constant Re_{θ}. However in this report, the integral length scale was used as opposed to the dissipation length scale.

Maciejewski and Moffat (1989) used a free-jet facility with a constant temperature plate positioned off-axis and several jet diameters downstream of the jet exit plane to generate turbulence levels as high as 60% with $\beta = 28$. The flow field in this case was also highly non-uniform. They found that there was a continual increase in the surface heat transfer and that their data best scaled with a new and simpler parameter, St', which uses the maximum rms

velocity in the near wall region. The St' parameter was determined to be independent of flow geometry and to be a function of turbulence level only.

Ames and Moffat (1990) studied both skin friction and heat transfer enhancement with high levels of freestream turbulence. Turbulence levels up to 20% were generated using a combustor simulator. They proposed a new correlating parameter, the TLR parameter, which is defined as

$$TLR = Tu \left(\frac{\Delta}{L_u^{\varepsilon}} \right)^{0.33} \left(\frac{\mathrm{Re}_{\Delta}}{1000} \right)^{0.25} \tag{1.2}$$

Ames and Moffat noted that defining the edge of a boundary layer with high freestream velocity is rather difficult and used integral quantities rather than boundary-layer thicknesses in defining the TLR parameter. In Equation 1.2, $\Delta = \theta$, (the momentum thickness) for shear stress enhancement while for heat transfer enhancement, $\Delta = \Delta_2$ (the enthalpy thickness). The TLR was considerable successful in scaling not only their own data but also the data of Maciejewski and Moffat.

Sahm and Moffat (1992) also studied the effects of freestream turbulence levels on heat transfer and skin friction. They used combinations of jets and grids to generate turbulence levels as high as 30%. Sahm and Moffat reported that both the β parameter and the TLR parameter were successful in correlating the skin friction and heat transfer enhancement.

The different studies on skin-friction and heat transfer enhancement have used a number of correlations, which have been derived and applied in a variety of ways. In the application of these correlations, some additional parameters have been added or interchanged such as the integral length scales and dissipation length scales. Such an interchange introduces questions about the reliability of the interpretation of the correlations because the integral length scales

and dissipation length scales have been shown to vary for different flow fields. Consistent scales are imperative if effective comparisons are to be made in order to establish correlations that best predict heat transfer or skin-friction enhancement.

Objective Of The Study

The first objective of the current effort, which is the focus of this thesis, is the refurbishment and qualification of the THTTF, which has been unused for about 10 years. Included is the upgrading of the Automatic Data Acquisition And Control System (ADACS). The original installation was interfaced with a Hewlett Packard 3054A microprocessor based ADACS controlled by a Hewlett Packard series 200 microcomputer via a Hewlett Packard Interface Bus (HP-IB). The upgrade consists of the same transducers rigged to the ADACS and controlled by a personal computer via a General Purpose Interface Bus (GPIB). A LabView (version 4.1) program was written to control the THTTF via the ADACS.

The general organization of this report is described below. Chapter II describes the experimental test facility in detail with its subsystems. Details of the measurement technique and calibration are provided in Chapter III. In Chapter IV, the results of the qualification tests are given. A brief summary and conclusions are given in Chapter V.

CHAPTER II

THE EXPERIMENTAL APPARATUS

General Description

The Turbulent Heat Transfer Test Facility (THTTF) is a closed-loop subsonic wind tunnel designed to investigate the heat transfer and fluid dynamic characteristics of turbulent boundary layer flow over smooth and rough surfaces. The preliminary design and analysis were done by Norton (1983) and was based on a similar facility at the Stanford University [Healzer (1974), Pimenta (1975) and Coleman (1976)].

The THTTF consists of a test section of 24 Nickel-plated aluminum plates, which are abutted together to form a continuous flat surface. Each plate can be individually heated to achieve the required thermal boundary condition. This boundary condition could be an isothermal wall, a constant wall heat flux condition, unheated starting length, or a step change in temperature. The experimental results are presented in the form of Stanton numbers versus Re_X, the Reynolds number based on the location of interest along the test surface. The Stanton number is obtained by performing an energy balance on each plate using the measured heat and fluid variables. The measurement techniques and parameters are discussed in Chapter III.

The THHTF can be described as a facility comprising of four systems: the air flow system, the plate system, the cooling water system, and the data acquisition system. Figure 2.1 shows a schematic of the general arrangement of the facility. A description of each system follows.

Air Flow System

The prime mover for the air flow system is a Buffalo Forge 45AW industrial blower with a rating of 198 cubic meters (700 cubic feet) per minute of air at a static pressure of 38.1 cm (15 in) of water. This blower can deliver velocities from 6 to 67 meters per second of air in the test section of the THTTF. The blower is driven by an 18.6 kilowatt (25 hp) Dynamatic motor (model ACM-280) equipped with an Eaton variable-speed eddy-current clutch drive. An overhead wooden duct of cross section 4-feet wide by 2-feet high is connected to the blower discharge by flexible couplings. This wooden duct is attached to the ceiling and has a 90 degree turn to connect to the inlet header via flexible couplings. Air arriving at the header is filtered through a linen cloth filter box before passing through the air/water fin-and-tube heat exchanger. The heat exchanger is used to control the air temperature as described in the cooling water system.

The THTTF is designed to deliver uniform velocity air at low turbulence intensity over the test section comprised of 24 plates. To maintain low turbulence levels in the test section, a 3.8 cm thick aluminum honeycomb with a cell length-to-diameter ratio of 6 and a series of four woven stainless steel screens are installed downstream of the heat exchanger. The air exiting the heat exchanger flows into a three-dimensional nozzle designed to smoothly accelerate the flow without separation at the nozzle inlet or outlet [Healzer, (1974)]. The nozzle is made from fiberglass and has a contraction area ratio of 19.8 to 1 with an 84 cm by 122 cm inlet and a 10 cm by 51 cm outlet.

Air at uniform velocity exiting the nozzle is tripped by a wooden strip that is 1mm high by 12mm wide and runs across the full duct width (51 cm) at the inlet of the test section. Earlier measurements at freestream air velocities of 12 to 58 meters per second indicate that the axial

velocity at the nozzle exit is uniform to within 0.5%, while freestream turbulence intensities measured 4 cm downstream of the nozzle exit were less than 0.4% and 0.3% at 3 meters per second and 61 meters per second, respectively [Chakroun, (1992)]. This uniform velocity, low turbulence intensity air flows over the test section and exits through an adjustable plexiglas diffuser and into a wooden, vaned diffuser. A series of screen inserts at the inlet of the wooden diffuser are used to produce a pressure drop and serve as a coarse control for the static pressure in the test section. The blower inlet plenum is connected to the discharge of the diffuser. Make up air is filtered and inducted into the inlet plenum through adjustable orifices to replace the air lost through leakage in the air passages. A flexible coupling connects the inlet plenum to the blower intake.

The flexible couplings are used to minimize mechanical vibrations in the test section by isolating the blower and motor, the main sources of vibration. Other features include a massive concrete pad with vibration damping feet on which the blower and motor are mounted. Flow induced vibrations are suppressed with the use of a wooden, cross-shaped vortex breaker inserted into the blower inlet plenum. Noise in the overhead duct, plenum and header is damped through the use of batt insulation covered by rigid fiberglass insulation board on these components.

The air heats up as it circulates through the wind tunnel. The temperature of the air is controlled using a cooling system, described in Section 2.4.

Test Section And Plate System

The cross section of the test section is shown in Figure 2.2. The test section has a rectangular cross section with the two sidewalls and top wall made from 1.3 cm thick, clear plexiglass. The test plates make up the bottom wall. The top wall is constructed in six sections

along the direction of flow. Each section is joined to the next by thin, hard rubber joints. This top wall design introduces a degree of freedom for adjusting the top wall to achieve the specific pressure distribution required over the test section. Instrument access holes are provided along the center of the top wall directly above the center of each plate and transversely at strategic locations across plates 1, 12, 23, and 24. When no instrument access is required, the holes are plugged with precision-machined plexiglass plugs.

Static pressure taps are located on the left sidewall, 2.5 cm above the test plates and spaced 10.2 cm apart, centered on the midpoint of each plate width. These pressure taps are used to determine and adjust the pressure gradient in the flow direction. For the case of zero pressure gradient, which is the focus of this work, the difference in static pressure between the tap on the second plate and all other taps was maintained at less than 0.0130 in of water at a freestream velocity of 43 m/s.

The Test Plates

The 24 precision machined nickel plated aluminum test plates form the bottom wall of the test section. The test plate is a composite assembly of four parts; the top plate, the resistance heater pad, an insulation pad, and an aluminum backing plate.

Each test plate assembly consists of a top plate that provides the test surface, which is 10.2 cm wide in the flow direction, 45.7 cm in the transverse direction and 0.95 cm thick. Beneath this top plate is a custom manufactured flexible resistance heater pad for heating of the plates. These pads are about 1.1 mm thick and provide uniform heat flux to the lower surface of each plate. The heaters are made by Watlow Electric Manufacturing Co. and are made from resistance wire spiraled around a glass cord sandwiched between two pieces of glass fabric coated with silicone rubber. Heat loss from the bottom of the assembly is minimized by

inserting an insulation pad between the heater and the aluminum backing plate. The backing plate provides structural rigidity for the plate and is fastened to the assembly by two screws. These screws are positioned and tightened to ensure proper contact between the top plate and the heater pad.

As shown in Figure 2.3, dowell pins are used to secure the plates together forming a continuous test surface 2.4 m long. The allowable step at each interface between two plates is 0.0013 cm. The smooth plates used in the qualification checks have a surface finish measured as less than 0.508 μm (20 micro inches).

The test plates are supported on precision straight edges that are thermally isolated from the steel side rails that provide the required structural support. In order to minimize conduction losses from the sides of the plates, these side rails are heated to about the same temperature as the plates and act as heated guard rails.

The plates are individually heated to obtain the required thermal boundary condition. Each plate has a motor driven variable voltage transformer which supplies the voltage to the heater pads of the corresponding plate and is used to control the temperature of each plate. Plate temperature is measured with two Fenwal UUT45J1 thermistors embedded in each plate.

Electrical power to all the heater circuits is supplied through a single Powermark-75110 A.C. voltage regulator, which is connected to the building service (110V). Power from this regulator is fed to the plates through Powerstat-15M21 motor driven variable transformers that are used for fine adjustment. These transformers are grouped in three banks of eight and each bank is supplied power through a Variac-W10 variable transformer. The three W10 variable transformers are manually set and used for coarse adjustment of each bank.

Cooling Water System

The temperature of the circulating air is controlled with the aid of an air to water heat exchanger. Figure 2.4 is a schematic of the cooling water loop, which consists of the following;

1. A 186 W (1/4 hp) Bell and Gossett pump (Model 1552)
2. A 150 gallon water storage tank with four depth sensing valves.
3. A Trane fin-and-tube heat exchanger with 4 rows of finned coils in the flow direction with a frontal area of 33 in by 48 in.
4. A ¾ in motorized drain ball valve, GF-Type 105.

Energy in the form of heat is added to the air as it passes through the blower and over the plates. The air is maintained at constant temperature by extracting heat from it as it flows through the heat exchanger before the air enters the nozzle at the inlet of the test section. The circulating cooling water picks up the heat extracted from the air. In order to keep a constant water temperature in the storage tank, some of the heat extracted from the air is dumped by bleeding off proportional amounts of water via the drain valve. Make up water is fed into the tank from the building supply, and the water volume in the tank is maintained at the desired level using four adjustable depth sensing valves.

Data Acquistion System

The data acquisition package comprises of a Hewlett Packard 3054A Automatic Data Acquisition and Control system (ADACS) and a National Instruments PCI-GPIB data acquisition card installed in a personal computer with a Pentium 133 MHz processor.

The ADACS includes an HP-3437A high-speed system voltmeter, a HP 3456A high-resolution digital voltmeter, a HP-3497A data acquisition/control unit, and two HP-3498A extenders with a number of special function plug-in assemblies.

Suryanarayana (1986) presents a detailed discussion of the ADACS and its application in the monitoring and control of the THTTF.

The THTTF is rigged with transducers that sense the operating conditions in the THTTF. The output signals from the transducers are measured by the HP 3456A voltmeter, and this information is relayed to the personal computer through the NI PCI-GPIB card. The THTTF is controlled by a National Instruments LabView Version 4.1 program which runs on the PC. By comparing the operating condition information with the required conditions set, the LabView program determines the correct response and sends the appropriate commands to the HP-3497A data acquisition/control unit. The ADACS is used to control the power supplied to the plate heaters, the cooling system dump valve, and the blower motor speed. When the desired steady-state equilibrium condition has been achieved, the LabView program controls the ADACS to perform the necessary data acquisition.

A description of some of the LabView acquisition and control programs is given in Appendix B. Figure B.1 is an algorithm for the main control loop while Figure B.2 is an algorithm for the data acquisition process on the THTTF. The channel directory is summarized in Table B.1.

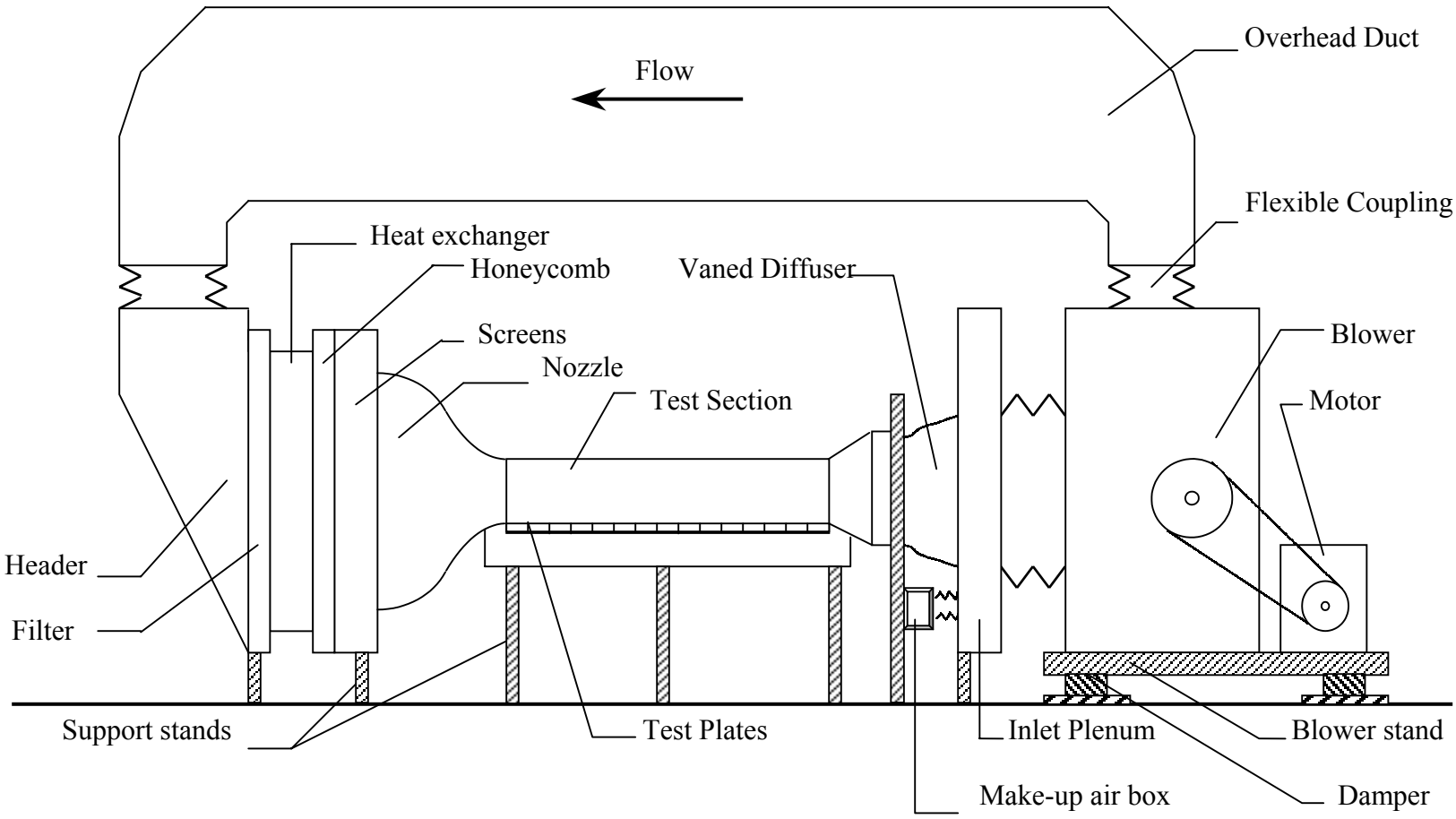

Figure 2.1 Schematic of the Turbulent Heat Transfer Test Facility (THTTF).

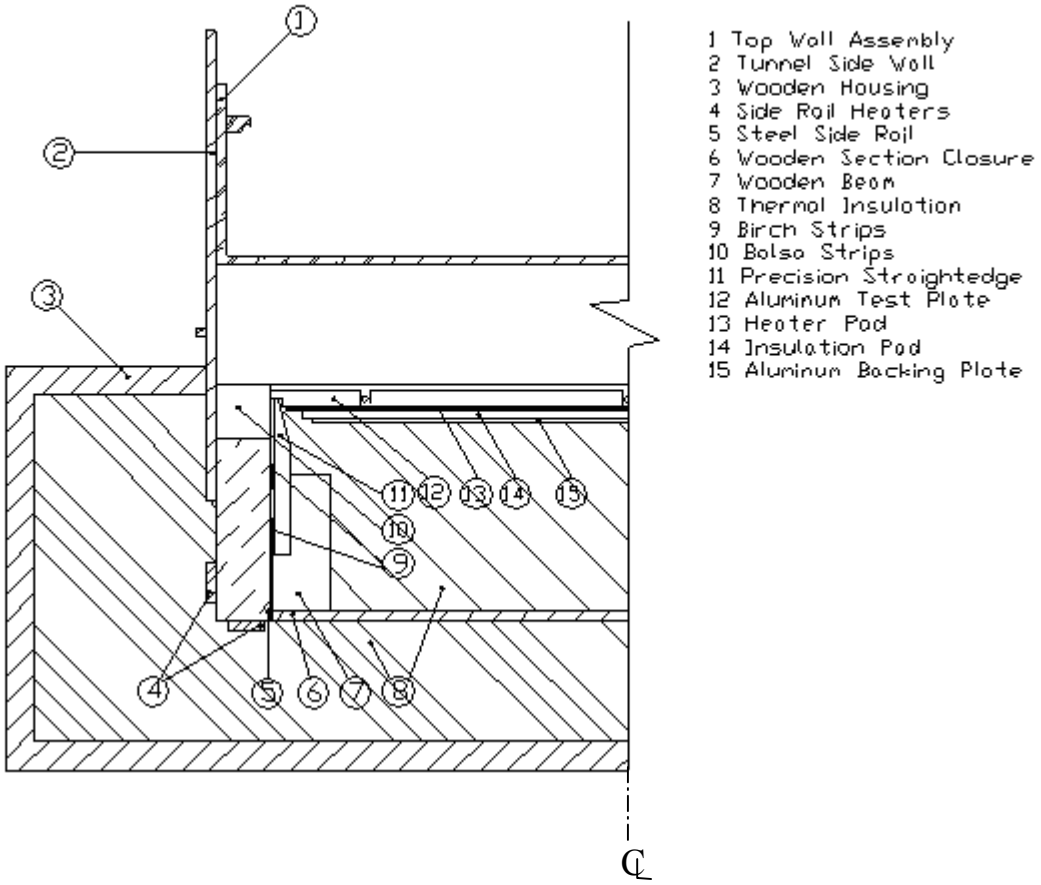

Figure 2.2 Cross section of the THTTF test section

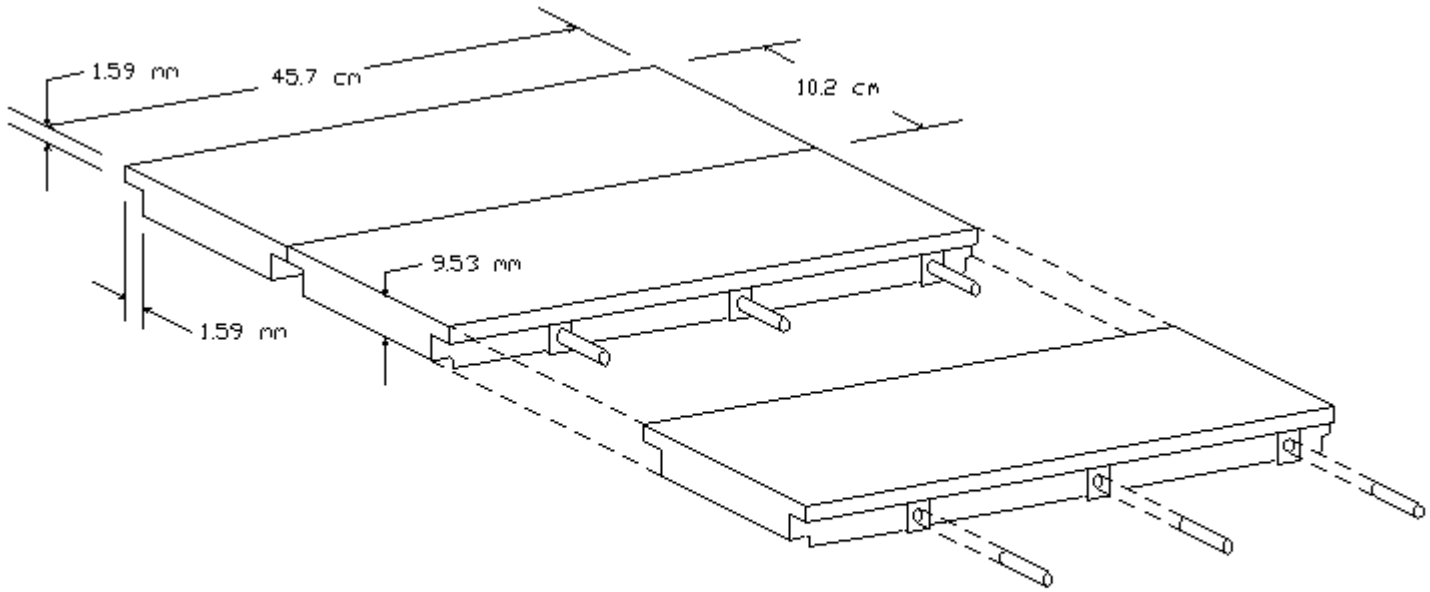

Figure 2.3 Schematic of the test plate assembly

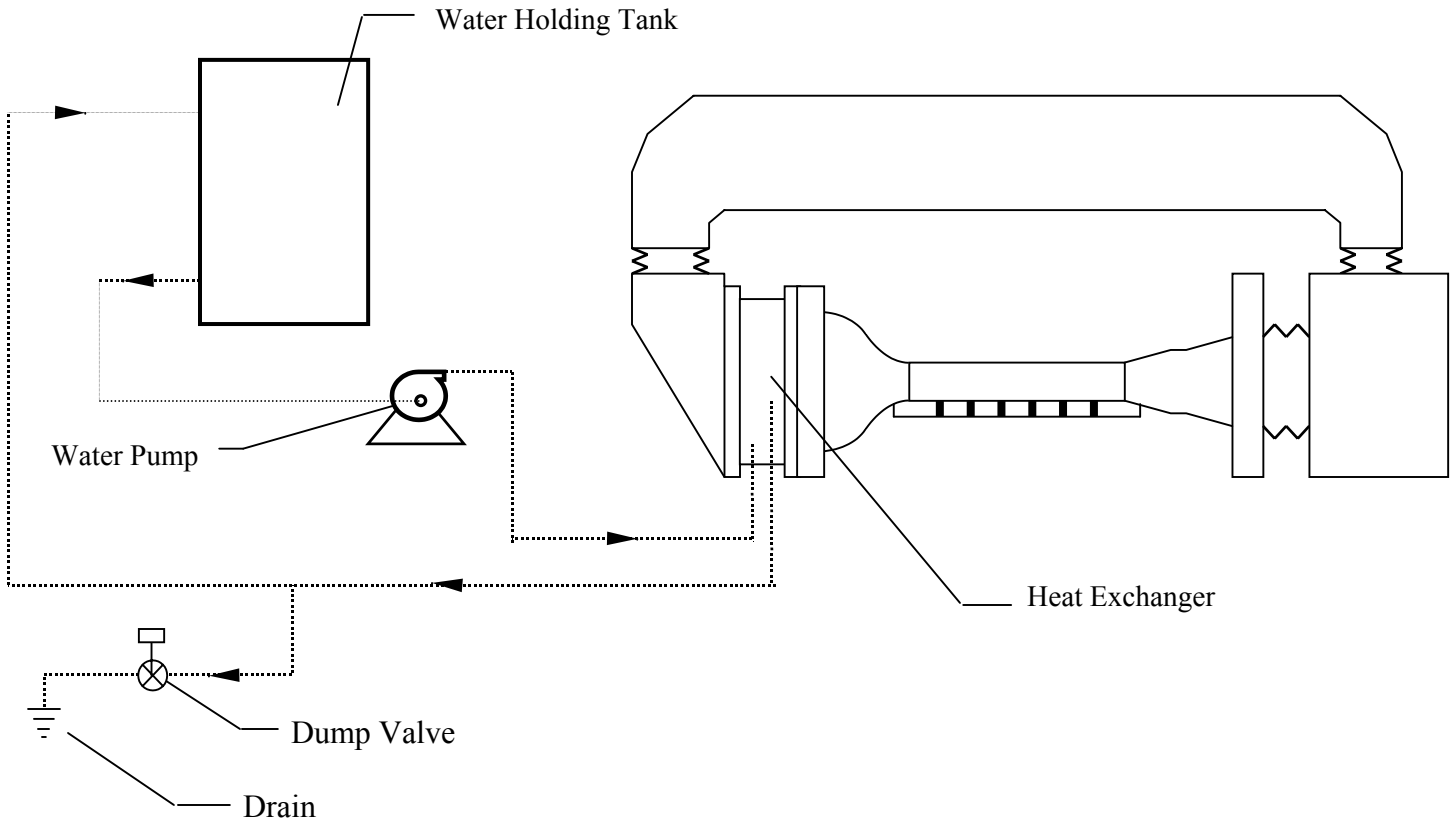

Figure 2.4 Schematic of the cooling water loop

CHAPTER III

MEASUREMENT TECHNIQUES AND CALIBRATION

Temperature

Plate temperature measurements are accomplished with the use of Fenwal Electronics type UUT45J1 thermistors. These are temperature sensitive resistors with a negative coefficient and a nominal value of 5000 ohms at 25 ^{o}C. Each heater plate has two thermistors embedded close to the plate surface through two small blind holes located at the bottom of the plate. These thermistors are guaranteed by the manufacturer to have an interchangeability of ± 0.2 ^{o}C over a standard range of temperatures from 0 ^{o}C to 70 ^{o}C. Although thermistors are extremely nonlinear, they are highly sensitive to small changes in temperature with sensitivities of about 1-2 kΩ/ ^{o}C. The freestream air temperature is also measured using the same type of thermistor.

The original calibration of the thermistors was achieved using a Blue M Model MR-3210A-1 constant temperature bath. The bath temperature was monitored by a Hewlett Packard Model 2804A quartz thermometer, which had a Model 1811A quartz probe installed. This thermometer has an absolute accuracy of ± 0.04 ^{o}C over a temperature range of –50 to 150 ^{o}C. Details of the calibration procedures are given in Brown (1988). Resistance measurements obtained by the ADACS is reduced to a temperature value using the Steinhart-Hart equation given below

$$\frac{1}{T[^{0}K]} = A + B\ln R + C(\ln R)^{3} \tag{3.1}$$

where R is the measured resistance in Ohms. A, B and C are curvefit constants and were calculated using the manufacturer's data as

A = 9.6401E-4

B = 2.1095E-4

C = 8.48E-8.

For this project, a Techne Inc. Model DB700A Block Calibrator was used to verify the calibration constants for a sample size of the thermistors. These constants were found to be essentially the same and thus the same calibration constants were employed in this report. However, calibration of the freestream air thermistor yielded the following constants

A = 9.805137E-4

B = 1.980149E-4

C = 1.753987E-7.

Power

Power is the single most important measurement required and its accuracy plays a major role in the reliability of the experimental results. The power input into the test plates is measured using an Ohio Semitronics Inc. Model EW5-B watt transducer. This is a high precision A.C. Watt transducer with an accuracy of ± 0.2% of reading as specified by the manufacturer. The Watt transducer generates a current output of 0-1 ma (dc) proportional to the input electrical power. This transducer has an input range of 0 – 500 W with the output of 1 ma corresponding to an input of 500 W.

The output from the transducer is measured by the ADACS. However, since the ADACS cannot measure current directly, the output signal is converted into a voltage and resistance signal by connecting a shunt resistance of 7.5 kΩ across the transducer output lines. The shunt

resistor was sized to compensate for the low current output from the transducer. The power input to each plate is determined by engaging the watt transducer in the plate heater circuit using automated switch closures (relays). The current output, which corresponds to the input power, is fed through the shunt resistor. The D.C voltage drop across the resistor and the resistance were then measured by the ADACS and converted to current and subsequently to a power reading using the calibration equation

$$P = 500 * I \tag{3.2}$$

where

P is the power in W

I is the current in mA

The watt transducer calibration was accomplished by comparing the transducer measurement to the actual power input obtained by measuring the resistance of the plate heaters and the A.C voltage drop across them. The power factor is required to account for the inductance of the plates during this measurement. Suryanarayana (1986) measured this power factor as 0.9997 to within ±1%, which is approximated to unity in this calibration.

Pressure / Velocity

Freestream velocity measurements are performed using a pitot static probe and a differential pressure transducer. The pitot probe is inserted into the freestream flow and the output, which is the difference between the total head and the static head, is fed into one of two Validyne Model P305D pressure transducers with ranges of 0.08 psi and 0.5 psi. The pressure transducer converts the input pressure differential into a 0-5 D.C voltage output proportional to the applied pressure difference. The ADACS measures the output signal from the transducer which have an accuracy of ± 0.5% of full scale as specified by the manufacturer.

The pressure transducers are calibrated against a Meriam Instruments Model 34FB2TM water micromanometer. This is an extremely sensitive 10 inch water micromanometer equipped with a magnifier to amplify the fluid meniscus at the reference hairline which provides a direct reading indication of 0.001″ of water. Each transducer was calibrated separately using 20 points within the transducer range. At zero pressure, both transducers exhibited a small but stable voltage output (zero shift). The data acquired were corrected for by subtracting the zero shift voltage from the transducer output voltage measurement. This corrected data were used to develop appropriate curvefit equations for the each transducer. Calibration curves for both the 0.08 psi and 0.5 psi transducers are shown in Figures 3.1 and 3.2, respectively.

The freestream velocity was evaluated from the reduction equation given below:

$$V = \sqrt{\frac{2\Delta P}{\rho}} \tag{3.3}$$

where

ΔP is the differential pressure output of the pressure transducer

ρ is the density of the ambient air at the prevailing barometric pressure

The density is obtained from the ideal gas law as

$$\rho = \frac{p}{RT} \tag{3.4}$$

where

p is the prevailing barometric pressure

R is the gas constant

T is the freestream air temperature

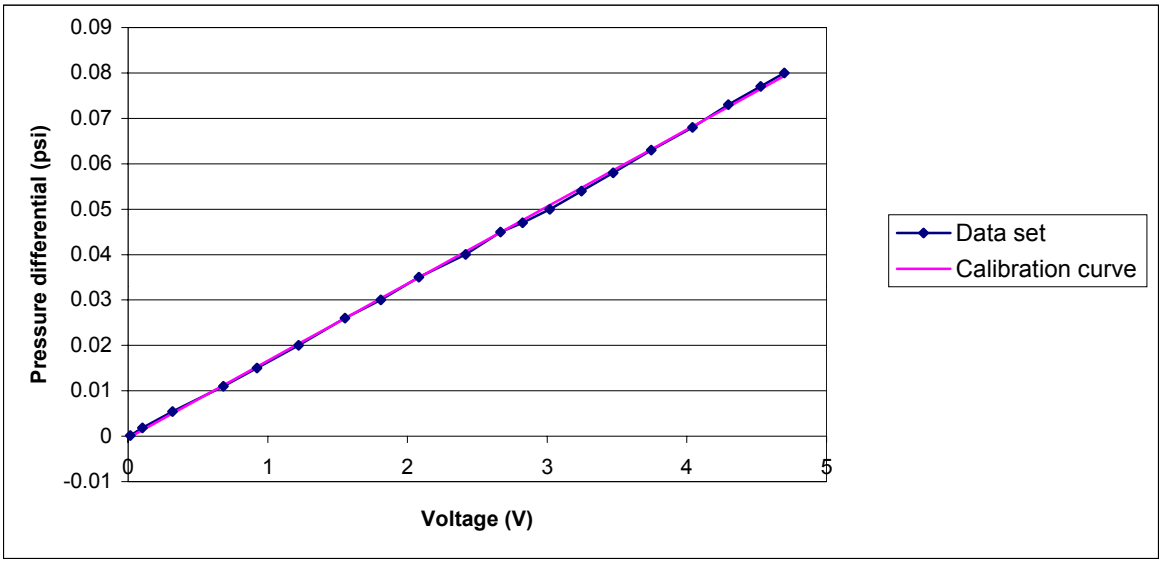

Figure 3 .1 Calibration curve for 0.08 psi transducer

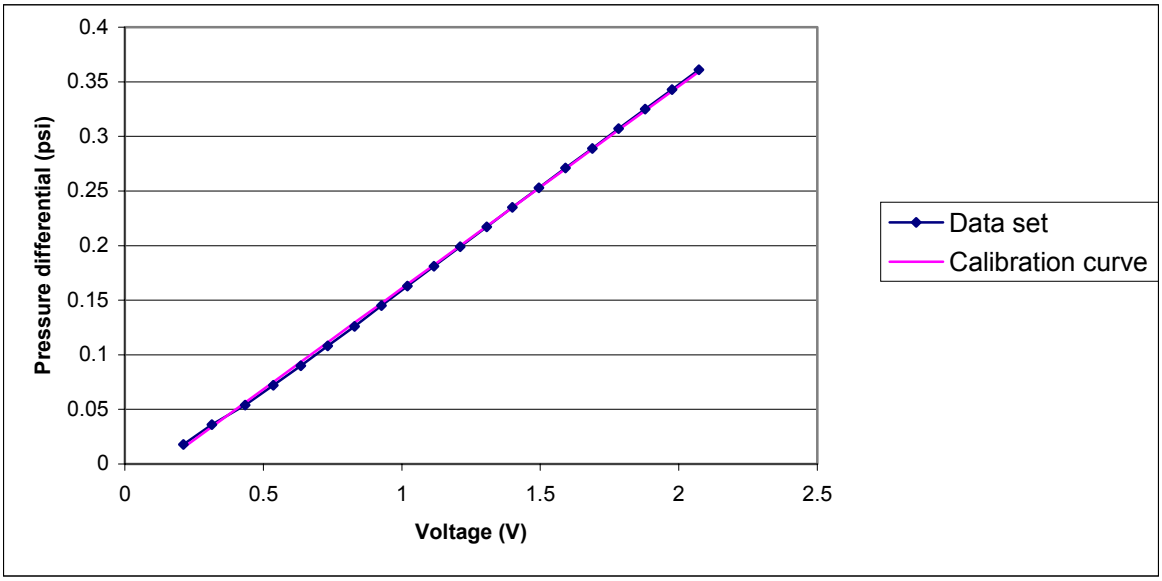

Figure 3.2 Calibration curve for 0.5 psi transducer

CHAPTER IV

QUALIFICATION TESTS

This chapter discusses the smooth wall qualification of the Turbulent Heat Transfer Test Facility. The objective of this qualification is to ascertain the fitness and ability of the installation to acquire accurate and reliable Stanton number data, to verify the correctness of the data reduction equations and data acquisition process, and to validate the control program for the ADACS.

Two levels of qualification were achieved for the THTTF. The first is a first-order replication comparison check that tests the repeatability or scatter in the results of a timewise experiment that is run more than once at a particular setpoint. The detailed uncertainty analysis of the facility suggests that the random errors in the experimental Stanton number determination are negligible compared to the systematic errors. Hence it is expected that the results obtained from replications on different days at a particular freestream velocity should produce data with negligible scatter. A successful first-order replication check is an indication that all factors influencing the random error of the experiment have been properly accounted for.

The second level is an *n*th-order replication level check that compares the Stanton number data obtained from the THTTF with previously published data from accepted sources. Agreement at an *n*th-order level can be taken as an indication that all significant contributors to the uncertainty in the experimental result have been accounted for.

Useful comparisons for the qualification check can only be made with results obtained using similar facilities with the same thermal and hydraulic boundary conditions. All

comparisons and data given in this report are for zero pressure gradient, isothermal wall temperature, incompressible boundary layer flow at a constant freestream velocity over an aerodynamically smooth flat surface without transpiration. These experiments were also conducted with low freestream turbulence with levels of order 2-5% recorded by Reynolds et al. (1958). Freestream turbulence levels in the order of 0.7% were recorded on a similar test stand at the Stanford University [Healzer (1974), Pimenta (1975) and Coleman (1976)].

Experimental determination of the Stanton number was based on an energy balance on each of the test plates. The details of this energy balance are given in Appendix A. Stanton number data reported on earlier studies using the THTTF were evaluated using a Stanton number definition based on the difference between the plate surface temperature and the total freestream temperature. However, the data for the experimental Stanton number generated by other studies referenced in this report for comparison are based on a Stanton number evaluated using the difference between the test surface temperature and the freestream recovery temperature. Love (1988) evaluated the difference in definitions and concluded that the differences in total and recovery temperatures are numerically insignificant for the range of velocities considered by the previous studies. He based his analysis on the similarity of the velocity and enthalpy fields and used analogies to show that it is consistent to base the Stanton number calculation on total temperature. The definition adopted in this report is consistent with that previously reported on studies conducted with the THTTF.

First-order Replication Level Check

The first-order replication level check compared Stanton number results replicated on different days at a particular set point for the freestream velocity. Figure 4.1 shows the replicated data at a freestream velocity of about 43 m/s. Three data sets are presented in Figure 4.1 and represent freestream velocities of 42.8 m/s, 42.9 m/s and 43.2 m/s which were taken

over a period of seven weeks. Figure 4.1 indicates that there is negligible scatter in the data, and this result is consistent with the detailed uncertainty analysis that suggests that any significant errors are systematic. Similar results were obtained for replications at freestream velocities of 60 m/s and 28 m/s.

*n*th-order Replication Level Check

The *n*th-order replication check was accomplished by comparing the THTTF smooth wall Stanton number data with previously reported and widely accepted data. The definitive data set for zero pressure gradient, isothermal wall temperature, incompressible boundary layer flow over smooth flat plates without transpiration are those of Reynolds, Kays and Kline (1958). The experimental facility used to generate this data is similar to the THTTF consisting of 24 individually heated plates. The plates were made of copper and had dimensions of 6.4 cm in the flow direction and 84 cm transverse to the flow providing a total test section length of 1.5 m. This installation produced freestream turbulence levels of 2 to 5 % depending on the freestream velocity. The Stanton number was determined by measuring the power input to each plate and making the appropriate corrections for conductive and radiation losses.

Coleman et al. (1988) successfully executed the smooth wall qualification of the THTTF. The data generated at that time were well accepted and for the purpose the *n*th-order check, this report will compare the data generated in that experiment to data from the current project. The values for Stanton and x-Reynolds number from the qualification check of Coleman et al (1988) are reported as part of the thesis by Brown (1988). Figure 4.2 is a comparison of previous data reported on the THTTF with the current data at a freestream velocity of 43 m/s. Similar results were obtained for freestream velocities of 28 m/s and 60 m/s as shown in Figures 4.3 and 4.4, respectively.

Other reliable smooth-wall data sets chosen for this *n*th-order check are those from a series of experiments at Stanford University. These experiments were conducted in a facility similar to the THTTF. The test section consisted of 24 individually heated plates with dimensions of 10.2 cm in the flow direction and 45.7 cm transverse to the flow. Freestream turbulence levels of 0.7% were recorded on the test apparatus. The Stanton number was evaluated by measuring the power input to each plate, the plate temperature, and the freestream recovery temperature. The data reduction process included correction for losses. These efforts by Moffat (1967), Kearney (1970) and Orlando (1974) reported data covering a freestream velocity range from 7 to 13.4 m/s and x-Reynolds number (Re_x) up to about 2 x10^6. Moffat (1967) performed his tests on this rig and correlated his Stanton vs. Re_x data with Equation 4.1. Figure 4.5 is a plot of samples from the Moffat data set.

$$St = 0.0286\left(\mathrm{Re}_x\right)^{-0.2}\left(\mathrm{Pr}\right)^{-0.4} \tag{4.1}$$

Figure 4.6 shows a plot of sample data from the data set of Reynolds, Kays and Kline while a composite plot for all data sets considered is shown in Figure 4.7. Figure 4.7 illustrates that about 95% of the data are enclosed in the ± 5% band indicating that the data correlates well with Equation 4.1. Figure 4.8 is a plot of the current data set at freestream velocity of 43m/s compared with Equation 4.1 and the ± 5% bands. This plot shows that all the new data set presented here are well within the ± 5% uncertainty band. Details of the uncertainty analysis in the experimental Stanton number determination for this apparatus are presented in Appendix A. Appendix C is a tabulation of the current data set.

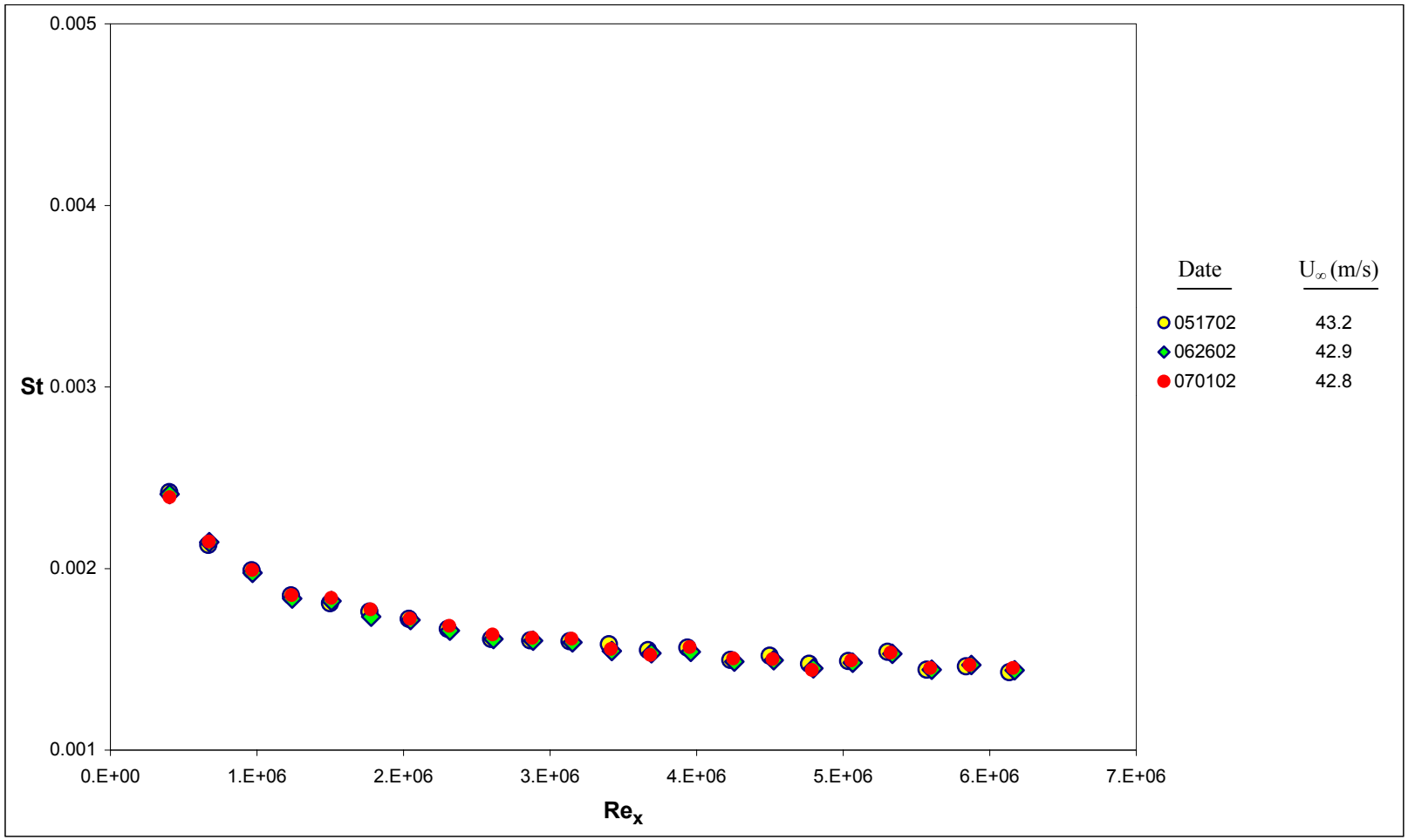

Figure 4.1 Stanton Number Data of Current Experiments at 43 m/s

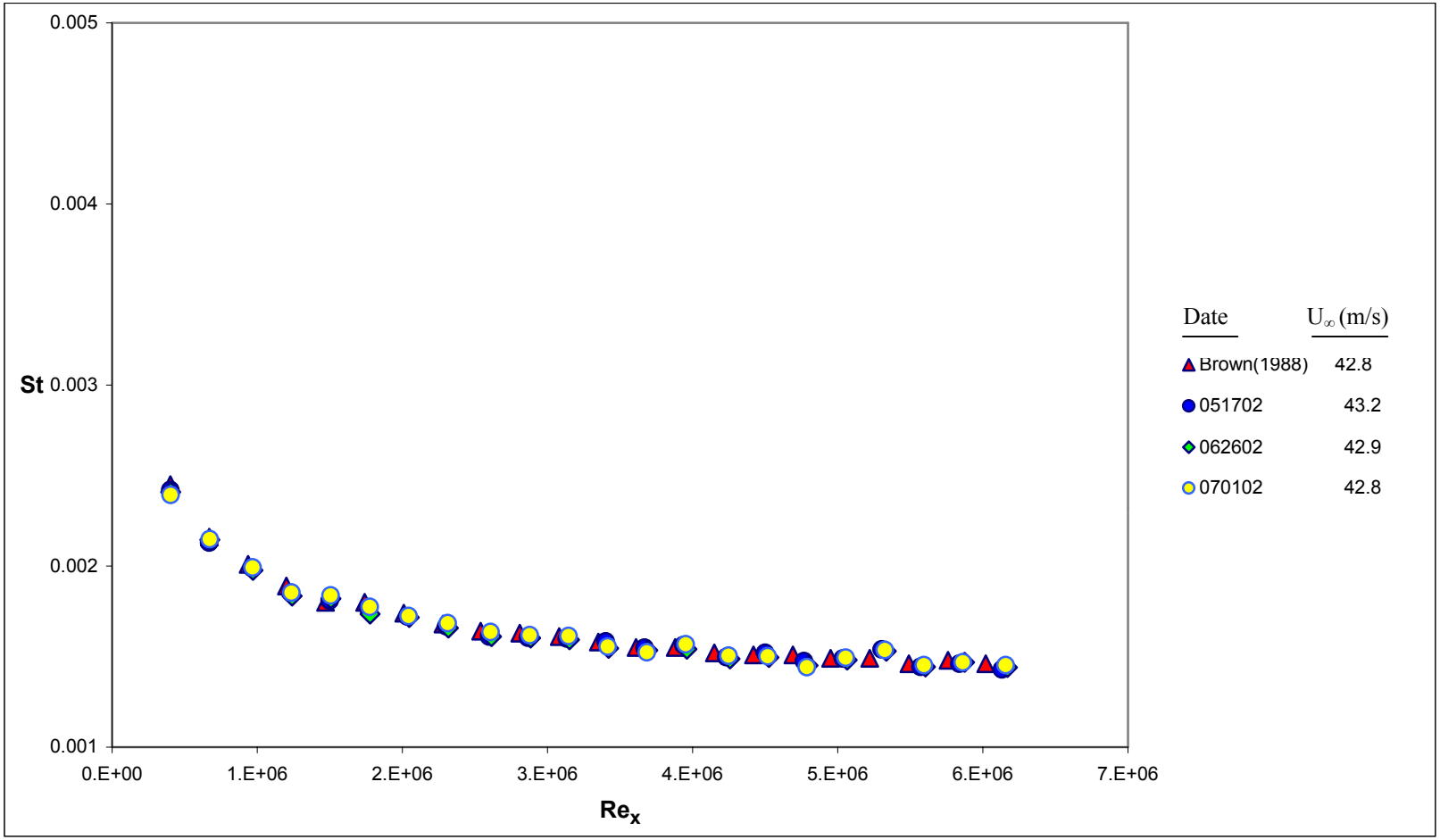

Figure 4.2 Stanton Number Data of Current Experiments at 43 m/s Compared with that of Brown (1988)

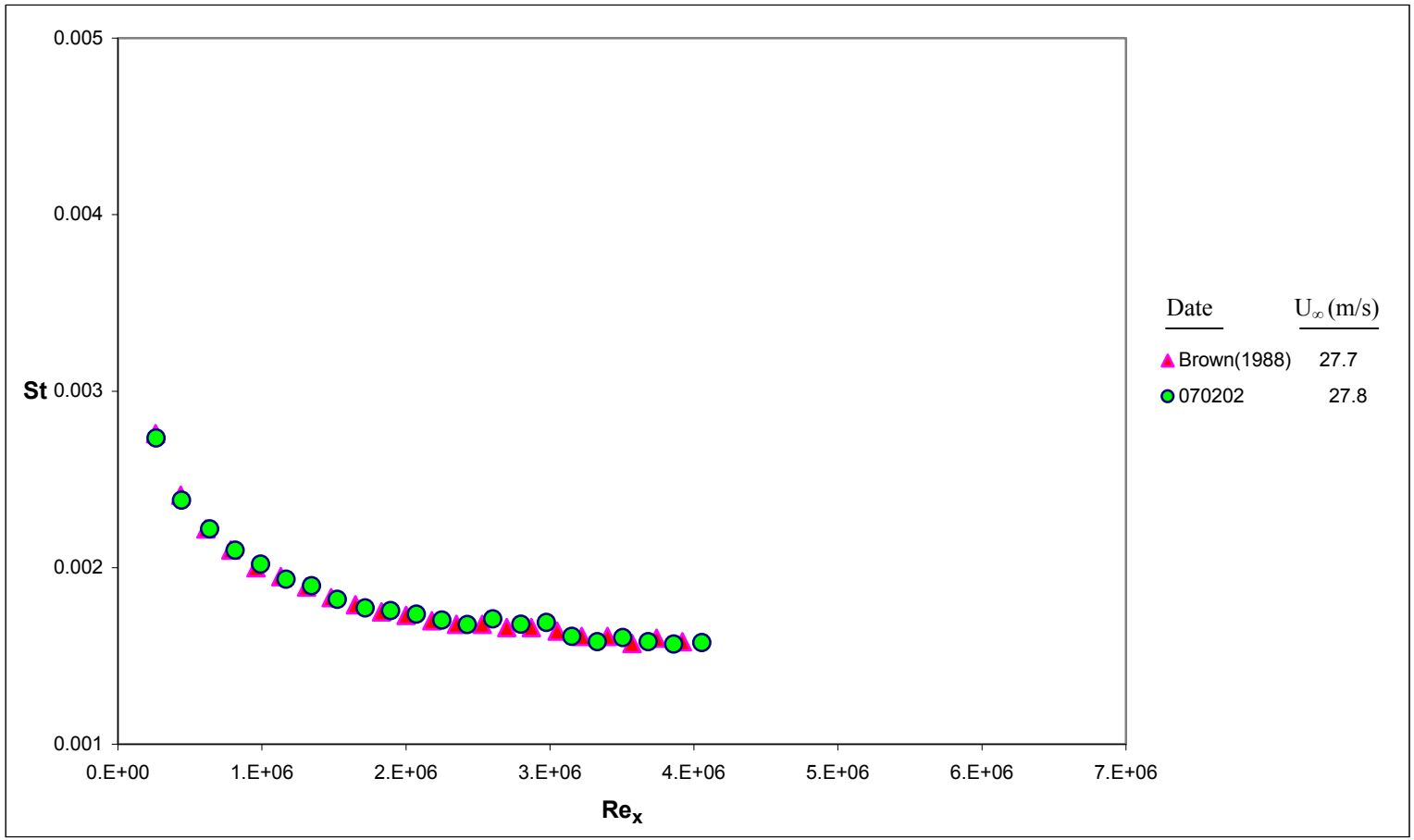

Figure 4.3 Stanton Number Data of Current Experiments at 28 m/s Compared with that of Brown (1988)

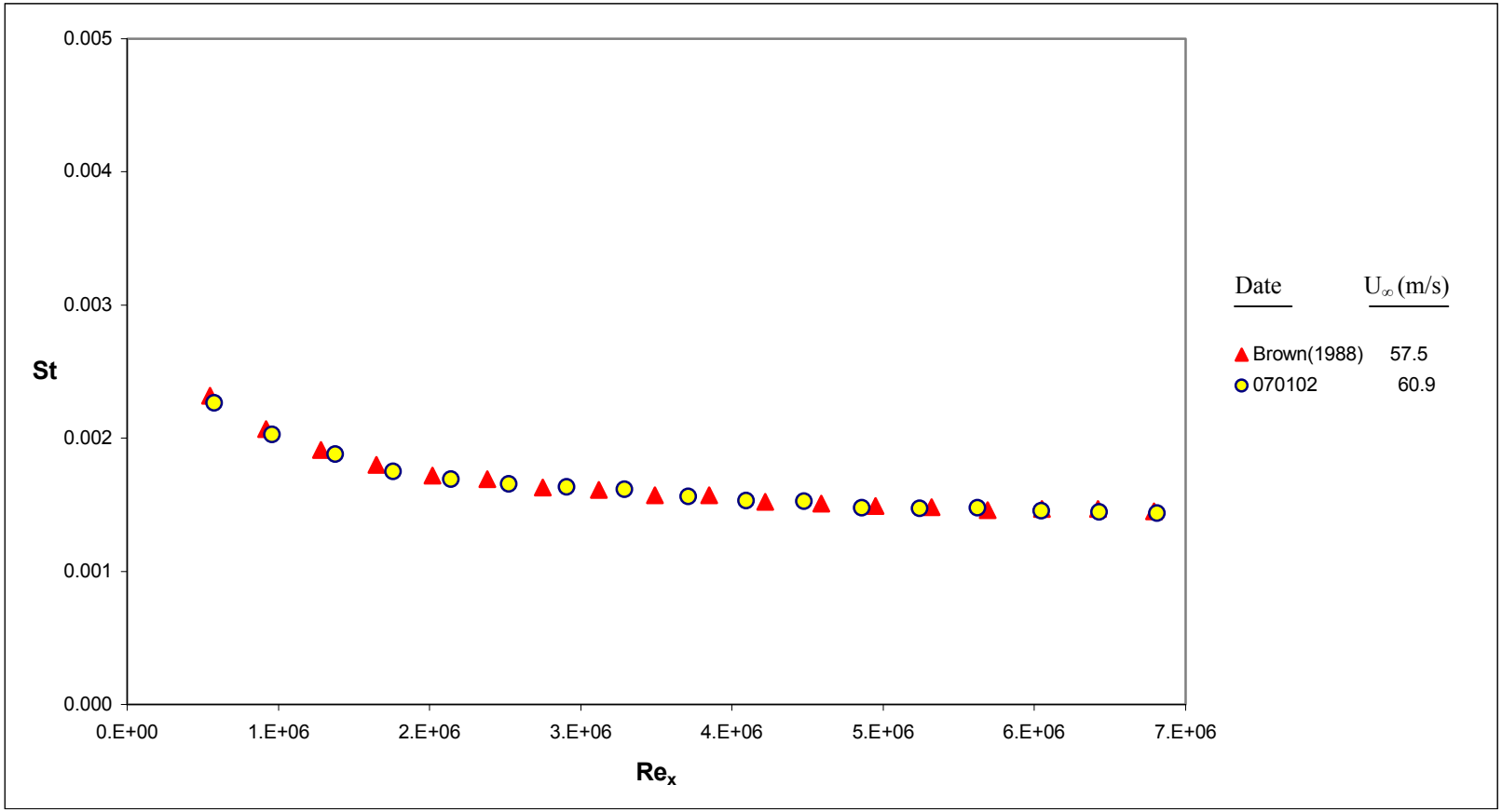

Figure 4.4 Stanton Number Data of Current Experiments at 60 m/s Compared with that of Brown (1988)

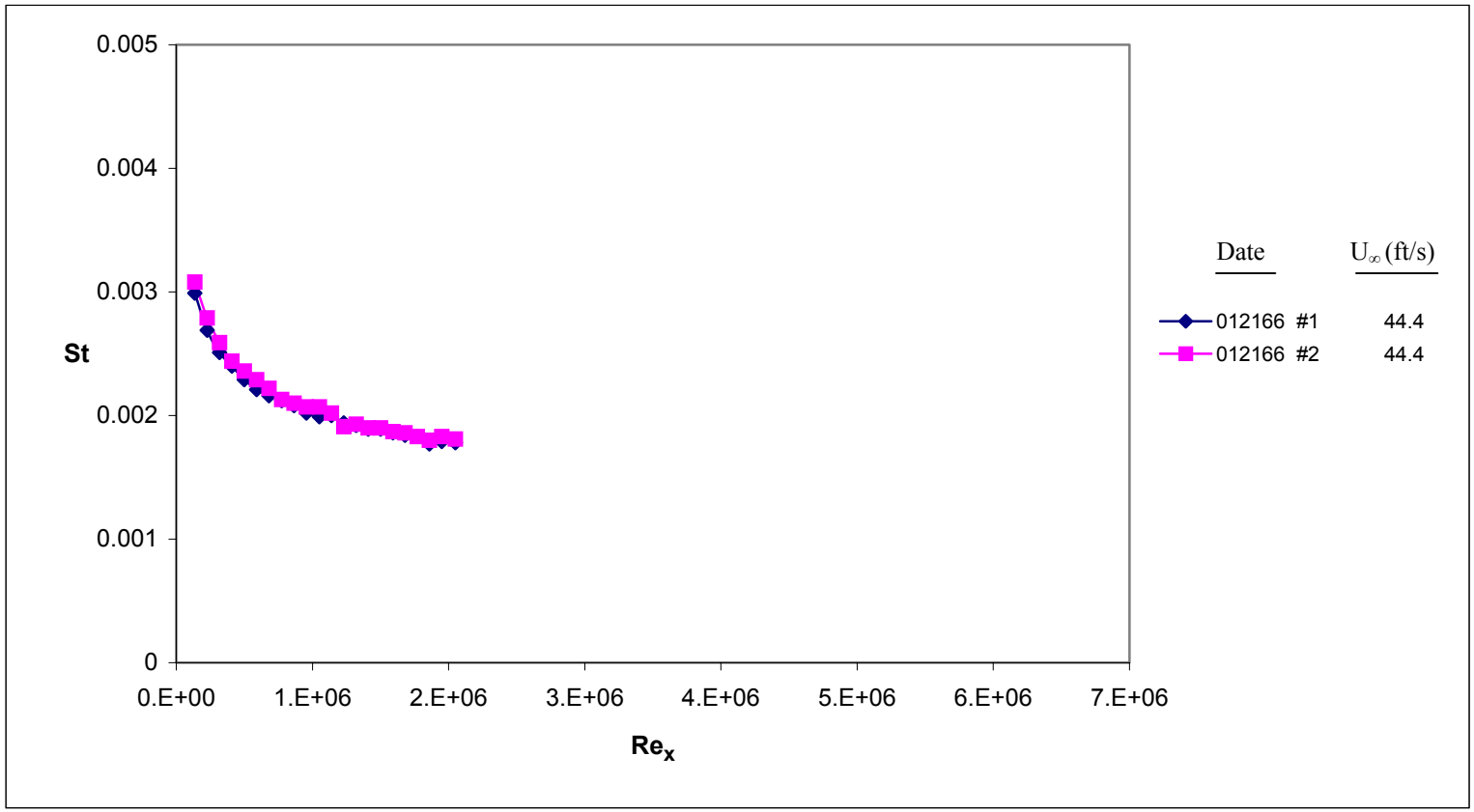

Figure 4.5 Samples from the Moffat (1967) Data Set at 44.4 ft/s.

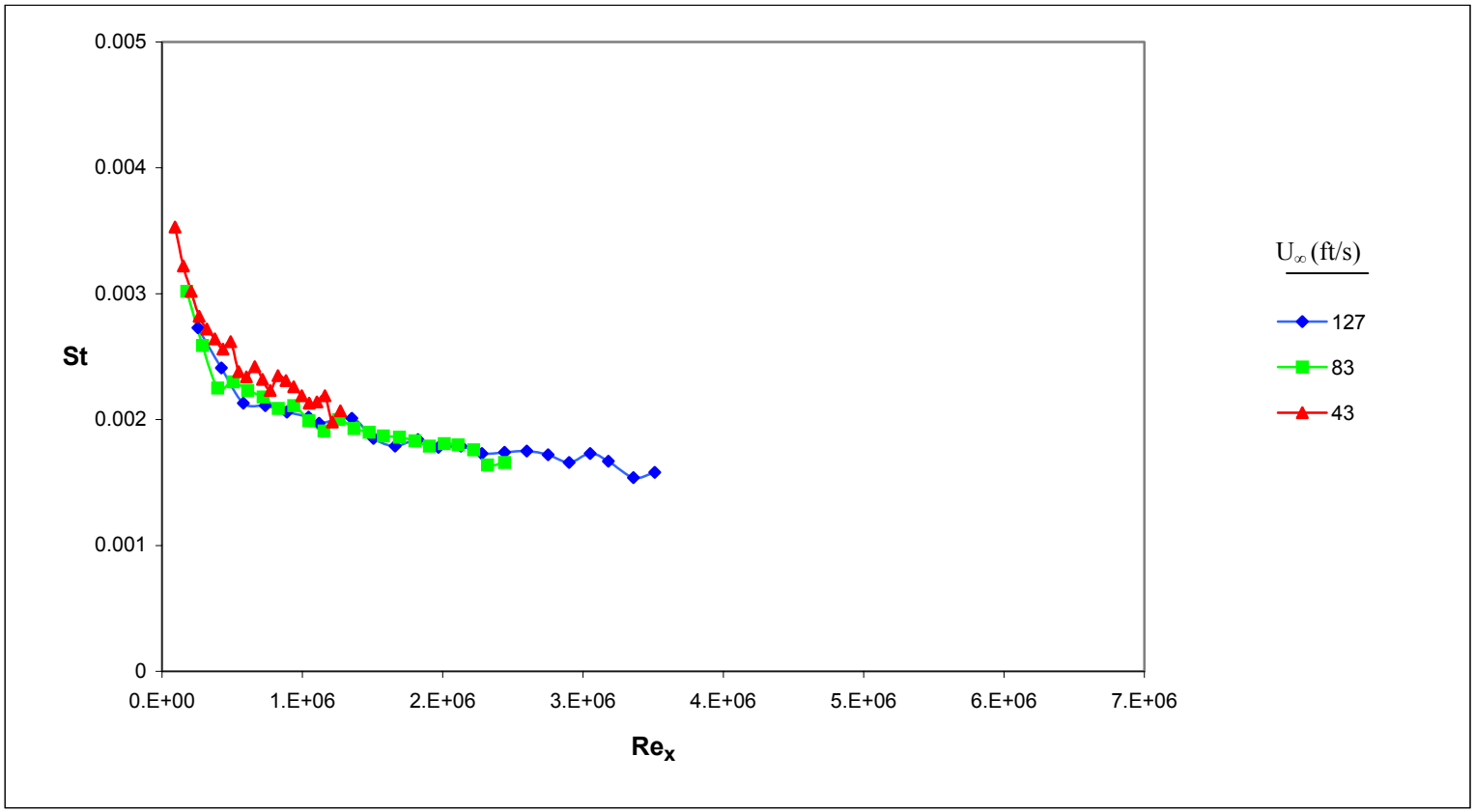

Figure 4.6 Samples from the Data Set of Reynolds, Kays and Kline (1958).

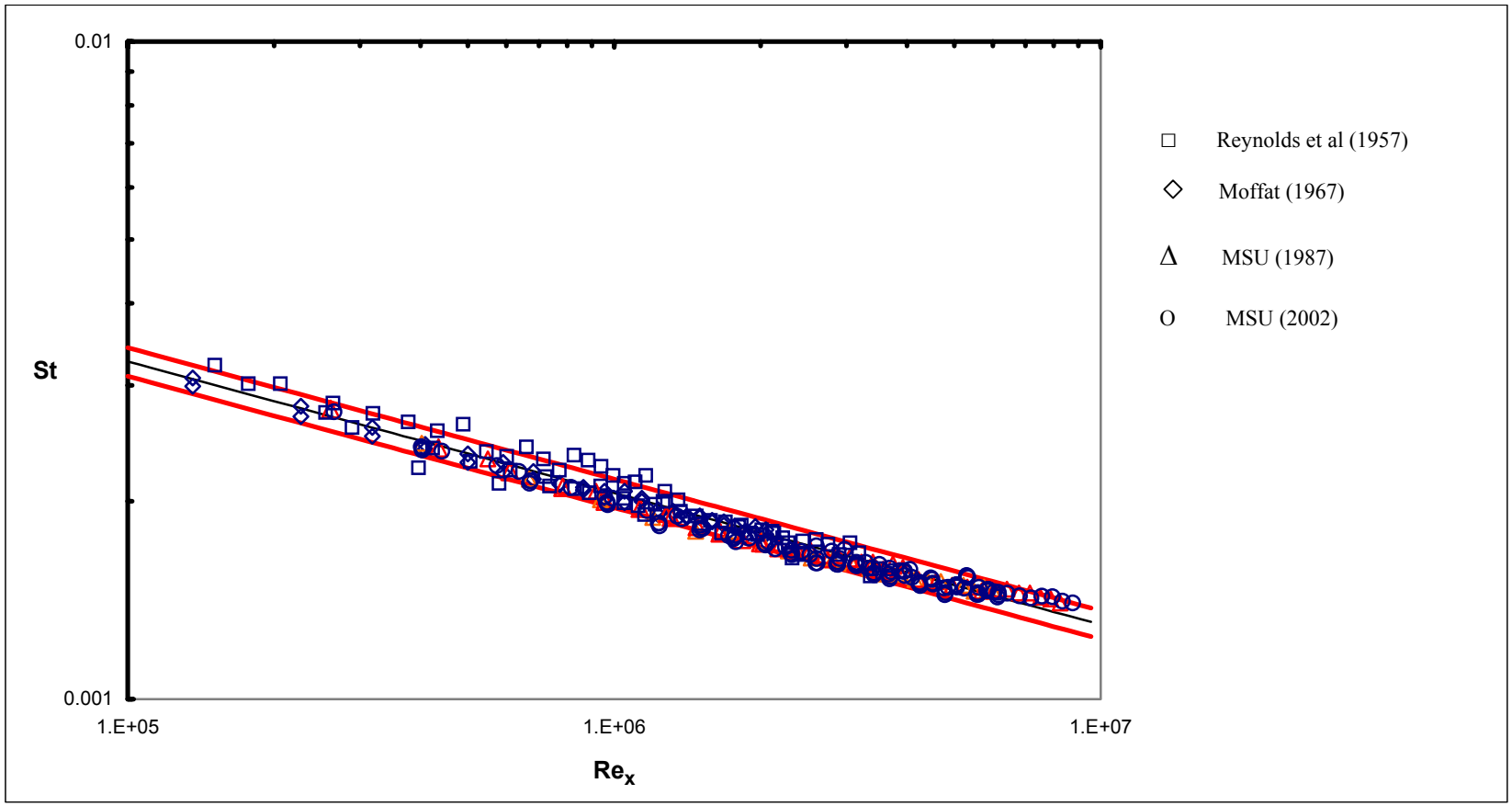

Figure 4.7 Composite Plot of All Stanton Number Data Considered vs x-Reynolds number

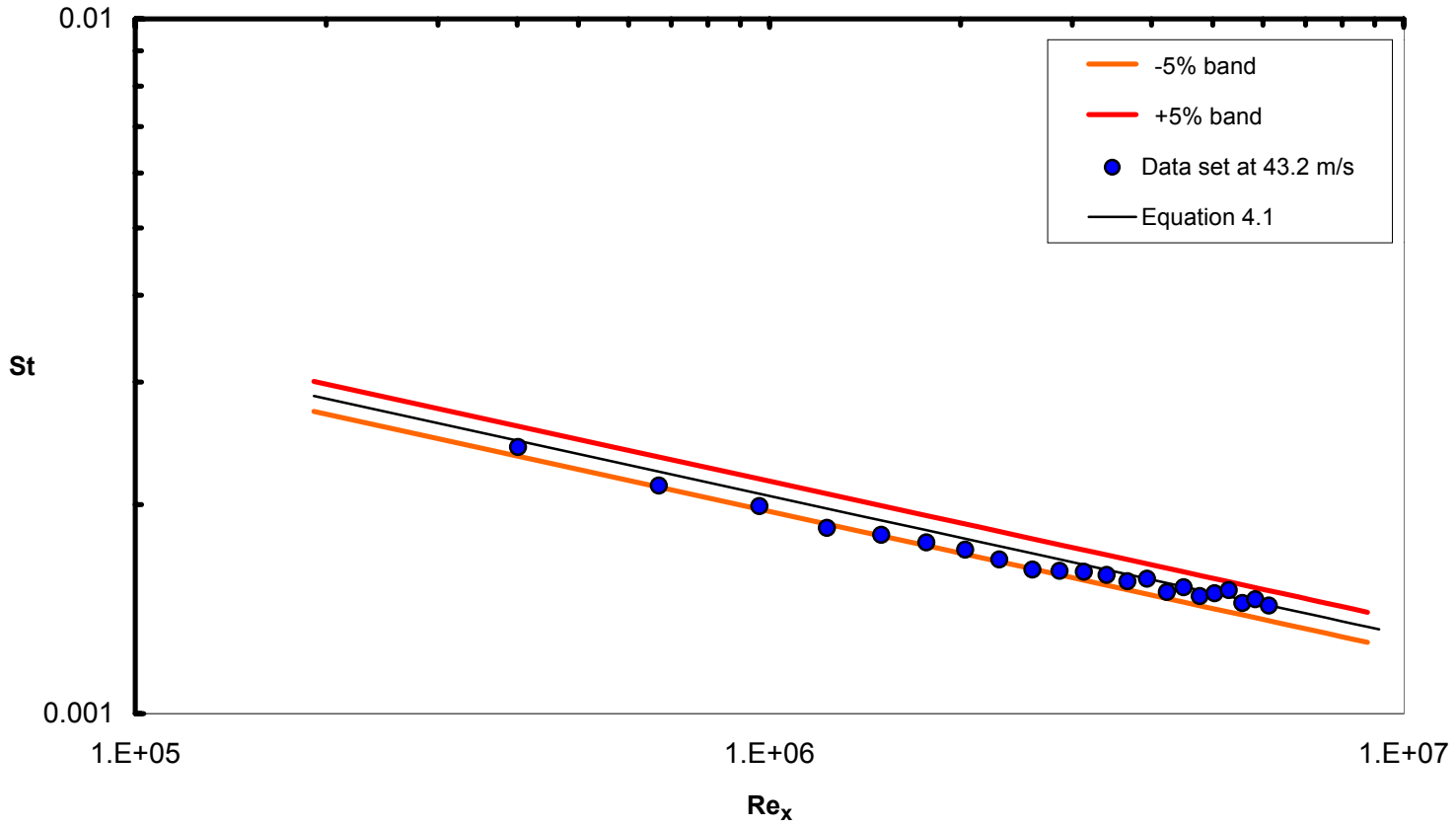

Figure 4.8 Stanton Number Data of Current Experiments at 43.2 m/s compared with the Moffat correlation.

CHAPTER V

SUMMARY AND CONCLUSIONS

The motivation for this work is the need to accurately predict the heat transfer characteristics of high freestream turbulent flow over rough surfaces. The Turbulent Heat Transfer Test Facility (THTTF) has been used in the past to generate well-accepted heat transfer data under different thermal and hydraulic boundary conditions. This facility has, however, remained unused for about 10 years. The focus of this project has been the refurbishment of the THTTF and the upgrading of the Automated Data Acquisition and Control System (ADACS).

Two levels of qualification checks were carried out in order to validate the proper functioning of the upgraded ADACS as well as verify the ability of the THTTF to produce acceptable heat transfer data. A first-order replication check was used to verify negligible scatter in the heat transfer data at speeds of 60, 43 and 27 m/s. An *n*th-order replication check established very good agreement between the heat transfer data reported by Brown (1988) and that from the current effort. Brown (1988) had compared and established agreement between his data set and those of Reynolds et al. (1958), Moffat (1967), Kearney (1970), and Orlando (1974). Thus, the present data set compare favorably with the definitive data sets that have previously been published and accepted. With the successful completion of these two replication checks, the conclusion is made that the upgraded programs, the measurement techniques and data reduction procedures are correct and that the GPIB interface is functioning properly.

Having completed the refurbishment and qualification checks, the THTTF is now set for the second phase of the project. This phase includes the design and installation of a turbulence generator and further experimental studies to determine the effects of high freestream turbulence on skin-friction and heat transfer enhancement.

REFERENCES

1. Ames, F.E., and Moffat, R.J., (1990), Effects of Simulated Combustor Turbulence on Boundary Layer Heat Transfer. AIAA/ASME Thermophysics and Heat Transfer Conference, Seattle, pp. 11-17.

2. Blair, M.F., (1983), Influence of Free-Stream Turbulence on Turbulent Boundary Layer Heat Transfer and Mean Profile Development, Part II – Analysis of Results. *Trans. ASME, Journal of Heat Transfer*, Vol. 105, pp. 33-40.

3. Brown, G. B (1988), Smooth Wall Qualification of a Turbulent Heat Transfer Test Facility. M.S. Thesis, Mechanical and Nuclear Engineering Department, Mississippi State University.

4. Castro, I.P., (1984), Effects of Freestream Turbulence on Low Reynolds Number Boundary Layer Flows. *Journal of Fluids Engineering*, Vol. 106, pp. 298-306.

5. Chakroun, W., (1992), Experimental Investigation of the Effects of Acceleration on Flow And Heat Transfer in the Turbulent Rough-Wall Boundary Layer. Ph.D Dissertation, Mechanical and Nuclear Engineering Department, Mississippi State University.

6. Coleman, H.W., (1976), Momentum and Energy Transport in the Accelerated Fully Rough Turbulent Boundary Layer. Ph.D Dissertation, Mechanical Engineering Department, Stanford University.

7. Coleman, H. W., and Steele, W. G., (1999), Experimentation and Uncertainty Analysis for Engineers. Wiley-Interscience, New York.

8. Coleman, H. W., Hodge, B. K., and Taylor, R. P. (1984), A Reevaluation of Schlichting's Surface Roughness Experiment. *Trans. ASME, Journal of Fluids Engineering*, Vol. 106, pp. 60-65.

9. Coleman, H. W., Hosni, M. H., Taylor, R. P., and Brown, G. B. (1988), Smooth Wall Qualification of a Turbulent Heat Transfer Test Facility. Report TFD-88-2, Mechanical and Nuclear Eng. Dept., Mississippi State University.

10. Coleman, H. W., Hosni, M. H., Taylor, R. P., and Brown, G. B. (1991), Using Uncertainty Analysis in the Debugging and Qualification of a Turbulent Heat Transfer Test Facility. *Experimental Thermal and Fluid Science,* **4**:673-683.

11. Hancock, P.E., and Bradshaw, P., (1983), The Effect of Free-Stream Turbulence on Turbulent Boundary Layers. *Trans. ASME, Journal of Fluids Engineering*, Vol. 105, pp. 284-289.

12. Healzer, J.M., (1974), The Turbulent Boundary Layer on a Rough Porous Plate: Experimental Heat Transfer with Uniform Blowing. Ph.D Dissertation, Mechanical Engineering Department, Stanford University.

13. Hosni, M.H., Coleman, H.W., Taylor, R.P., (1989), Measurement and Calculation of Surface Roughness Effects on Turbulent Flow and Heat Transfer. Report TFD-89-1, Mechanical and Nuclear Engineering Department, Mississippi State University.

14. James, C.A., Hodge, B.K., and Taylor, R.P., (1993), A Discrete Element Method For The Prediction Of Friction And Heat Transfer Characteristics OF Fully-Developed Turbulent Flow In Tubes With Rib Roughness. Turbulent Enhanced Heat Transfer, HTD, Vol 239, pp 9-18.

15. Johnson, P. L., and Johnston, J. P., (1989), Active and Inactive Motionss in a Turbulent Boundary Layer – Interactions With Free-Stream Turbulence. Presented at the Seventh Symposium on Turbulent Shear Flows, Stanford University.

16. Kearney, D. W., (1970), The Turbulent Boundary Layer: Experimental Heat Transfer With Strong Favorable Pressure Gradients and Blowing. Ph.D Dissertation, Mechanical Engineering Department, Stanford University.

17. Kestin, J., (1966), The Effect of Free-Stream Turbulence on Heat Transfer Rates. *Advances in Heat Transfer*, 3, ed. by T.F. Irvine and J.P. Harnett, Academic Press, London, 1.

18. Koutmos, P., and McGuirk, J.J., (1989), Isothermal flow in a Gas Turbine Combustor – a Benchmark Experimental Study. *Experiments in Fluids*, Vol. 7, p. 344.

19. Maciejewski, P. K., and Moffat, R. J., (1989), Heat Transfer With Very High Free-Stream Turbulence: Part I – Analysis of Results. *Trans. ASME, Journal of Heat Transfer*, Vol. 114, pp. 834-839.

20. MacMullin,R., Elrod, W., and Rivir, R., (1989), Free-Stream Turbulence from a Circular Wall Jet on a Flat Plate Heat Transfer and Boundary Layer Flow. Trans. *ASME, Journal of Turbomachinery*, Vol. 111, pp. 78-85.

21. Moffat, R.J., (1967), The Turbulent Boundary Layer on a Porous Plate: Experimental Heat Transfer with Uniform Blowing and Suction. Ph.D Dissertation, Mechanical Engineering Department, Stanford University.

22. Moody, L.F., (1944), Friction Factors for Pipe Flow. *Trans. ASME*, Vol. 66, pp.671-678.

23. Nikuradse, J., (1933), Stromungsgesetze in Rauhen Rohren. VDI- Forchungsheft 361. (Also Laws of Flow in Rough Pipes. NACA TM 1292).

24. Norton, B.A., (1983), Preliminary Analysis and Design of a Turbulent Heat Transfer Test Apparatus. M.S. Thesis, Mechanical and Nuclear Engineering Department, Mississippi State University.

25. Orlando, A.F., (1974), Turbulent Transport of Heat and Momentum in a Boundary Layer Subject to Deceleration, Suction and Variable Wall Temperature. Ph.D Dissertation, Mechanical Engineering Department, Stanford University. (Also Report HMT-17).

26. Pimenta, M.M., (1975), The Turbulent Boundary Layer: An Experimental Study of the Transport of Momentum and Heat with the Effect of Roughness. Ph.D Dissertation, Mechanical Engineering Department, Stanford University.

27. Reynolds, W. C., Kays, W. M., and Kline, S. J. (1958), Heat Transfer in the Turbulent Incompressible Boundary Layer-Constant Wall Temprerature. NASA TM 12-1-58W, Washington D.C.

28. Sahm, M.K., and Moffat, R.J., (1992), Turbulent Boundary Layers With High Turbulence: Experimental Heat Transfer and Structure on Flat and Convex Walls. Stanford University, Report HMT-45.

29. Schlichting, H., (1936), Experimentelle Untersuchungen zum Rauhigkeits-problem. *Ingenieur-Archiv*, vol. VII, No. 1, pp. 1-34. (Also "Experimental Investigation of the Problem of Surface Roughness," NACA TM 823).

30. Seidman, M.H., (1978), Rough Wall Heat Transfer in a Compressible Turbulent Boundary Layer. AIAA Paper No. 78-163.

31. Simonich, J. C., and Bradshaw, P., (1978), Effect of Free-Stream Turbulence on Heat Transfer through a Turbulent Boundary Layer. *Trans. ASME, Journal of Heat Transfer*, Vol. 100, pp. 671-677.

32. Suryananarayana, P. V. R., (1986), Remote Data Acquisition and Control Techniques for Wind and Water Tunnel Experiments. M.S. Thesis, Mechanical and Nuclear Engineering Department, Mississippi State University.

33. Taylor, R. P., Coleman, H. W., and Hodge, B. K., (1989), Prediction of Heat Transfer in Turbulent Flow Over Rough Surfaces. *Trans. ASME, Journal of Heat Transfer*, Vol. 111, pp. 568-572.

34. Taylor, R. P., Love, P. H., Coleman, H. W., and Hosni, M. H. (1990), Step Heat Flux Effects on Turbulent Boundary Layer Heat Transfer. *Journal of Thermophysics*, Vol 4, pp. 121-123.

35. Thole, K. A., (1992), High Freestream Turbulence effects on Turbulent Boundary Layers. Ph.D Dissertation, University of Texas at Austin, Turbulence and Turbine Cooling Research Laboratory.

36. Thole, K. A., and Bogard, D. G. (1995), Enhanced Heat Transfer and Shear Stress Due to High Free-Stream Turbulence. *Trans. ASME, Journal of Turbomachinery*, Vol. 117, pp. 418-424.

APPENDIX A

UNCERTAINTY ANALYSIS

Evaluation of the Experimental Stanton Number

The Stanton number is a dimensionless convective heat transfer coefficient and is often used as an alternative for the Nusselt number. The Stanton number is defined as

$$St = \frac{Nu}{RePr} \tag{A.1}$$

Substituting for the definitions of Nusselt number, Reynolds number, and Prandtl number, the Stanton number can be written as

$$St = \frac{h}{\rho C_p U_\infty} \tag{A.2}$$

where

Nu	is the Nusselt number
Pr	is the Prandtl number
Re	is the Reynolds number
h	is the convective heat transfer coefficient
ρ	is the density of the freestream air
C_p	is the specific heat of the freestream air
U_∞	is the freestream air velocity

The convective heat transfer rate from the test plate surface to the air q, is defined as

$$q = hA\left(T_p - T_o\right) \tag{A.3}$$

where

A	is the test plate area
T_p	is the test plate surface temperature
T_o	is the total temperature of the freestream air

In order to accurately determine the convective heat transfer rate at the test surface it is necessary to account for conduction and radiation losses. This is accomplished by applying a steady state energy balance to the each test plate. Figure A.1 shows this energy balance which is expressed as equation A.4.

$$W = q + q_c + q_r \tag{A.4}$$

where

W is the power supplied to the plate

q_c is the conductive heat loss rate

q_r is the radiation heat loss rate

The conductive and radiation losses are modeled as equations A.5 and A.6, respectively. The details of the development of the models used to estimate the conductive and radiation losses are discussed in subsequent sections.

$$q_c = (UA)_{eff}(T_p - T_{rail}) \tag{A.5}$$

$$q_r = \sigma \varepsilon A(T_p^4 - T_r^4) \tag{A.6}$$

Solving equation A.3 for h and equation A.4 for q and then substituting into equation A.2 yields equation A.7, which is the form of the data reduction equation used in the evaluation of the experimental Stanton number.

$$St = \frac{W - q_r - q_c}{A\rho C_p U_\infty (T_p - T_o)} \tag{A.7}$$

The final form of the data reduction equation used for the evaluation of the Stanton number is obtained by expressing the Stanton number as a function of all the variables. Substitution of equations A.5 and A.6 into equation A.7 yields

$$St = \frac{W - \sigma \varepsilon A(T_p^4 - T_r^4) - (UA)_{eff}(T_p - T_{rail})}{A\rho C_p U_\infty (T_p - T_o)} \tag{A.8}$$

Heat Loss Models

The conduction heat loss rate from the plates was modeled by experimentally determining the effective conductances between each test plate and the adjoining plates and the metal support rails. The effective plate-to-plate conductance was minimized to a negligible level by maintaining the plates at an isothermal condition. The effective conductance between the plate and the support rail was determined by laying insulation over the entire test surface and heating the plates up to a constant temperature. The plates were also insulated on the bottom sides. Hence there was negligible radiative or convective heat loss. A steady-state energy balance requires that the total input power to each heater plate is equal to the conductive heat transfer loss from each plate. The effective conductance $(UA)_{eff}$ was determined from equation A.5.

The radiation heat loss was modeled using a gray body enclosure radiation model. This is because the test plates are enclosed by cast clear acrylic sheet sidewalls and topwall. Clear cast acrylic has a high absorptivity and will transmit only 2% of the incident infrared radiation [Russel (1980)]. The radiative loss from the test plate surface was estimated as equation A.6.

The details of the assumptions and uncertainties related with the models used for estimating the conduction and radiative losses are provided by Brown (1988).

Detailed Uncertainty Analysis

The methods employed in the detailed uncertainty analysis follow the procedures discussed by Coleman and Steele (1999), which are consistent with the ANSI/ASME Standard on Measurement Uncertainty. A brief statement of the procedure is that the true value of a quantity that is approximated by an experimental result r lies within the interval $r \pm U_r$ with 95% confidence. This is expressed mathematically in equation A.9.

$$U_r = \left(B_r^2 + P_r^2\right)^{\frac{1}{2}} \tag{A.9}$$

Where

U_r is the uncertainty in the result

B_r is the bias limit of the result

P_r is the precision limit of the result

The bias limit is an estimate of the magnitude of the fixed, constant errors. The precision limit is an estimate of the scatter in results caused by random errors and unsteadiness and is defined such that the $\pm P_r$ interval about a result is the estimate of the band within which 95% of such results would fall if the experiment were repeated many times under the same conditions and with the same equipment.

For a result that is a function of J variables and parameters X_i, the functional equation can be written as

$$r = r\,(X_1, X_2, X_3, \ldots\ldots\ldots, X_J) \tag{A.10}$$

Equation A.8 is such a result for the experimental Stanton number St. Equation A.8 expresses the Stanton number explicitly in most of the variables involved in the Stanton number determination. However, additional variables are used in the calculation of the static and total temperatures of the freestream air as well as in the moist air property calculations used in the evaluation of the specific heat and density. The total and static temperatures of the freestream air are calculated from equations A.11 and A.12, respectively, using the recovery temperature measured by the thermistor probe and a recovery factor for the probe.

$$T_o = T_r + (1 - r)\left(\frac{U_\infty^2}{2C_p}\right) \tag{A.11}$$

$$T_\infty = T_r - r\left(\frac{U_\infty^2}{2C_p}\right) \tag{A.12}$$

where

T_o is the total temperature of the freestream air

T_∞ is the static temperature of the freestream air

r is the recovery factor for the thermistor probe (r = 0.86)

These additional variables not expressed here and their contributions to the overall uncertainty are discussed in the corresponding sections for the uncertainty in the measured variables by Coleman et al. (1991) and Taylor (1991).

The propagation of the precision limits P_{X_i} of the measured variables into the result is given by

$$P_r = \left[\sum_{i=1}^{j} \left(\frac{\partial r}{\partial X_i} P_{X_i} \right)^2 \right]^{1/2} \tag{A.13}$$

and the propagation of the bias limits B_{X_i} of the variables into the result is given by

$$B_r = \left\{ \left[\sum_{i=1}^{j} \left(\frac{\partial r}{\partial X_i} B_{X_i} \right)^2 \right] + 2 \left(\frac{\partial r}{\partial X_1} \right) \left(\frac{\partial r}{\partial X_2} \right) B'_{x_1} B'_{x_2} + \ldots\ldots\ldots \right\}^{1/2} \tag{A.14}$$

The second term on the right hand side of equation A.14 represents the contribution to the bias limit of two variables that are perfectly correlated. As discussed by Coleman and Steele (1999), there is a similar term for each pair of variables (X_1 and X_2) for which portions (B'_{x_1} and B'_{x_2}) of the bias limits arise from the same elemental error source. During the calibration of the thermistors used in the measurement of the plate, rail, freestream air and exit water

temperatures, the same standard was employed. Hence, a portion of the bias limit for each thermistor is perfectly correlated with a portion of the bias limits of the other thermistors.

During the design of the THTTF, it was estimated that the results obtained from experiments using this facility would be bias dominated, with negligible precision limit. This estimation was based on factors, which include the level of computer control achievable using the ADACS. It was expected that a "tight" steady state could be achieved thus minimizing any process unsteadiness. Another factor was the experience of Coleman (1976) in similar experiments using a comparable facility. These estimates have been proven to be true in a number of qualification checks by Coleman et al (1988), Brown (1988) and Coleman et al (1991). All these experiments report that

$$P_{st} \approx 0 \qquad \text{(A.15)}$$

However there is an exception to equation A.13 at low freestream velocities ($U_\infty \leq 12$ m/s). At these velocities the heat transfer coefficients are low and the time constant of the THTTF is large enough that a tight steady state is difficult to maintain because of fluctuations in the line voltage to the plate heater circuits. Another contributing factor is the fluctuation in the temperature of the cooling water. A 95% confidence estimate of $P_{st} = 3\%$ was determined for these conditions by observing the results for 8 replications at a freestream velocity of 12 m/s and 3 replications at 6 m/s [Coleman et al. (1988)]. This uncertainty in the Stanton number is present at low velocities due to system unsteadiness and not because of measurement uncertainty.

Application of equation A.14 to equation A.8 gives the bias limit of the Stanton number, B_{st}, as equation A.16.

$$
\begin{aligned}
B_{St}^2 = & \left(\frac{\partial St}{\partial T_p}\right)^2 B_{T_p}^2 + \left(\frac{\partial St}{\partial T_r}\right)^2 B_{T_r}^2 + \left(\frac{\partial St}{\partial T_{rail}}\right)^2 B_{T_{rail}}^2 + \left(\frac{\partial St}{\partial T_{wb}}\right)^2 B_{T_{wb}}^2 \\
& + \left(\frac{\partial St}{\partial P_{bar}}\right)^2 B_{P_{bar}}^2 + \left(\frac{\partial St}{\partial W}\right)^2 B_W^2 + \left(\frac{\partial St}{\partial U_\infty}\right)^2 B_{U_\infty}^2 + \left(\frac{\partial St}{\partial r}\right)^2 B_r^2 \\
& + \left(\frac{\partial St}{\partial A}\right)^2 B_A^2 + \left(\frac{\partial St}{\partial C_{p,air}}\right)^2 B_{C_{p,air}}^2 + \left(\frac{\partial St}{\partial C_{p,water}}\right)^2 B_{C_{p,water}}^2 \\
& + \left(\frac{\partial St}{\partial (UA)_{eff}}\right)^2 B_{(UA)_{eff}}^2 + \left(\frac{\partial St}{\partial \varepsilon}\right)^2 B_\varepsilon^2 + 2\left(\frac{\partial St}{\partial T_p}\right)\left(\frac{\partial St}{\partial T_r}\right) B'_{T_p} B'_{T_r} \\
& + 2\left(\frac{\partial St}{\partial T_w}\right)\left(\frac{\partial St}{\partial T_{rail}}\right) B'_{T_w} B'_{T_{rail}} + 2\left(\frac{\partial St}{\partial T_r}\right)\left(\frac{\partial St}{\partial T_{rail}}\right) B'_{T_r} B'_{T_{rail}}
\end{aligned}
\tag{A.16}
$$

Table A.1 represents the summary of the bias limits and nominal values for each variable as determined by previous efforts with the THTTF. Details of the procedures used for estimation and a detailed description of the bias limits are provided by Coleman et al. (1988) and Hosni et al. (1989).

Table A.1 Bias Limit and Nominal Value for Each Variable

Variable	Bias Limit	Nominal Value
Plate temperature, T_w	0.14 ^{o}C	45 ^{o}C
Rail temperature, T_{rail}	0.4 ^{o}C	45 ^{o}C
Recovery temperature, T_r	0.10 ^{o}C	30 ^{o}C
Wet-bulb temperature, T_{wb}	1.0 ^{o}C	27 ^{o}C
Barometric pressure, P_{bar}	1.0 mmHg	760 mmHg
Recovery factor, r	0.09	0.86
Power, W	0.9%	20-150 W
Area, A	0.03%	464.5 cm2
Freestream air velocity, U_∞	0.4%	6-70 m/s
Specific heat for air, $C_{p,\,air}$	0.5%	1.006 kJ/(kg.^{o}C)
Specific heat for water vapor, $C_{p,\,water}$	0.5%	1.86 kJ/(kg.^{o}C)
Effective conductance, $(UA)_{eff}$	45%	0.42 W/ ^{o}C
Emissivity, ε	45%	0.11

Final Uncertainty

The overall uncertainty associated with the Stanton number calculation is determined by evaluating equation A.16. Values for the partial derivatives are obtained using the nominal values and bias limits provided for each parameter.

Previous work on the THTTF employed the use of a jitter program to approximate the partial derivatives using a finite difference scheme. Details of the procedure are reported by Coleman et al. (1991), Taylor (1991), and Chakroun (1992). The final values reported for the uncertainty in the Stanton number in those experiments ranged from 2 to 5% depending on flow conditions. Table A.2 is a tabulation of typical values for uncertainty estimates in the experimental Stanton number for the current data set. From Table A.2 the uncertainty is in the range 1.9 to 2.5 %.

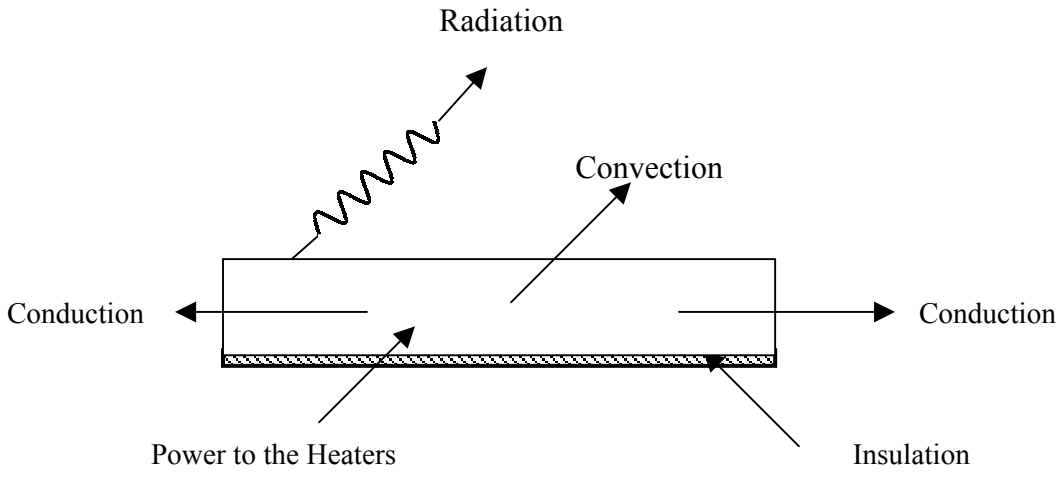

Figure A.1 Energy Balance on a Test Plate

Table A.2 Experimental Stanton Number Uncertainty

Date	U_{inf}	Plate #	T_P (°C)	T_{rail} (°C)	P (W)	Q_c (W)	Q_r (W)	St	U_{st}/St (%)
7/2/2002	27.8	2	44.2	46.5	69.6	-0.95	0.58	0.00273	1.9
		5	44.2	45.9	53.8	-0.70	0.58	0.00210	2.1
		10	44.3	46.9	45.1	-1.10	0.58	0.00177	2.2
		15	44.4	46.2	44.0	-0.76	0.59	0.00171	2.3
		20	44.4	46.3	41.2	-0.81	0.59	0.00160	2.3
		23	44.2	43.7	41.2	0.22	0.58	0.00157	2.4
6/26/2002	42.9	2	44.7	47.7	82.3	-1.25	0.54	0.00241	2.0
		5	44.5	47.8	61.4	-1.40	0.53	0.00183	2.1
		10	44.6	48.3	53.9	-1.58	0.53	0.00161	2.2
		15	44.7	47.8	52.1	-1.33	0.54	0.00154	2.2
		20	44.7	48.0	51.9	-1.38	0.54	0.00153	2.2
		23	44.7	45.6	49.8	-0.36	0.54	0.00144	2.3
7/1/2002	60.9	2	44.4	51.6	85.8	-3.01	0.48	0.00223	2.3
		5	44.2	51.6	64.7	-3.08	0.47	0.00172	2.4
		10	44.4	51.3	58.4	-2.89	0.48	0.00153	2.4
		15	44.5	50.6	56.7	-2.56	0.48	0.00147	2.4
		20	44.2	50.8	53.9	-2.76	0.47	0.00143	2.5
		23	44.1	47.9	53.1	-1.58	0.47	0.00140	2.5

APPENDIX B

LABVIEW CONTROL PROGRAMS

The following pages are a description of the LabView control and data acquisition programs or VIs (Virtual Instruments). Figure B.1 is an algorithm for the control of the THTTF, and Figure B.2 depicts the algorithm for data acquisition on the THTTF. Table B.1 is a summary of the channels as assigned on the HP-3497A data acquisition/control unit.

The pages that follow after Table B.1 describe each of the important VIs employed in the control and data acquisition. The general layout of the pages includes the VI name followed by five subheadings as described below.

1. Inputs: This is a listing of the required input to run the VI
2. Outputs: This is a listing of output information obtained from the VI
3. Sub VIs: These are the names of the subroutines (sub VIs) called by the VI
4. Caller VIs: These are the VIs that call the named VI as a sub VI
5. Description: This is a brief description of the operation and purpose of the VI.

Appendix B ends with a listing of VIs which have been modified from the original VI provided by National Instruments as part of the drivers for the HP-3054A system. The VIs are modified to suit the particular needs of the control and data acquisition programs and are renamed by appending a WT or W_T (for Wind Tunnel) at the beginning of the name. Some VIs like the WTvoltmeter.vi have a letter appended to the end, e.g., WTvoltmeter_T.vi to represent the voltmeter.vi VI that was modified for a temperature reading.

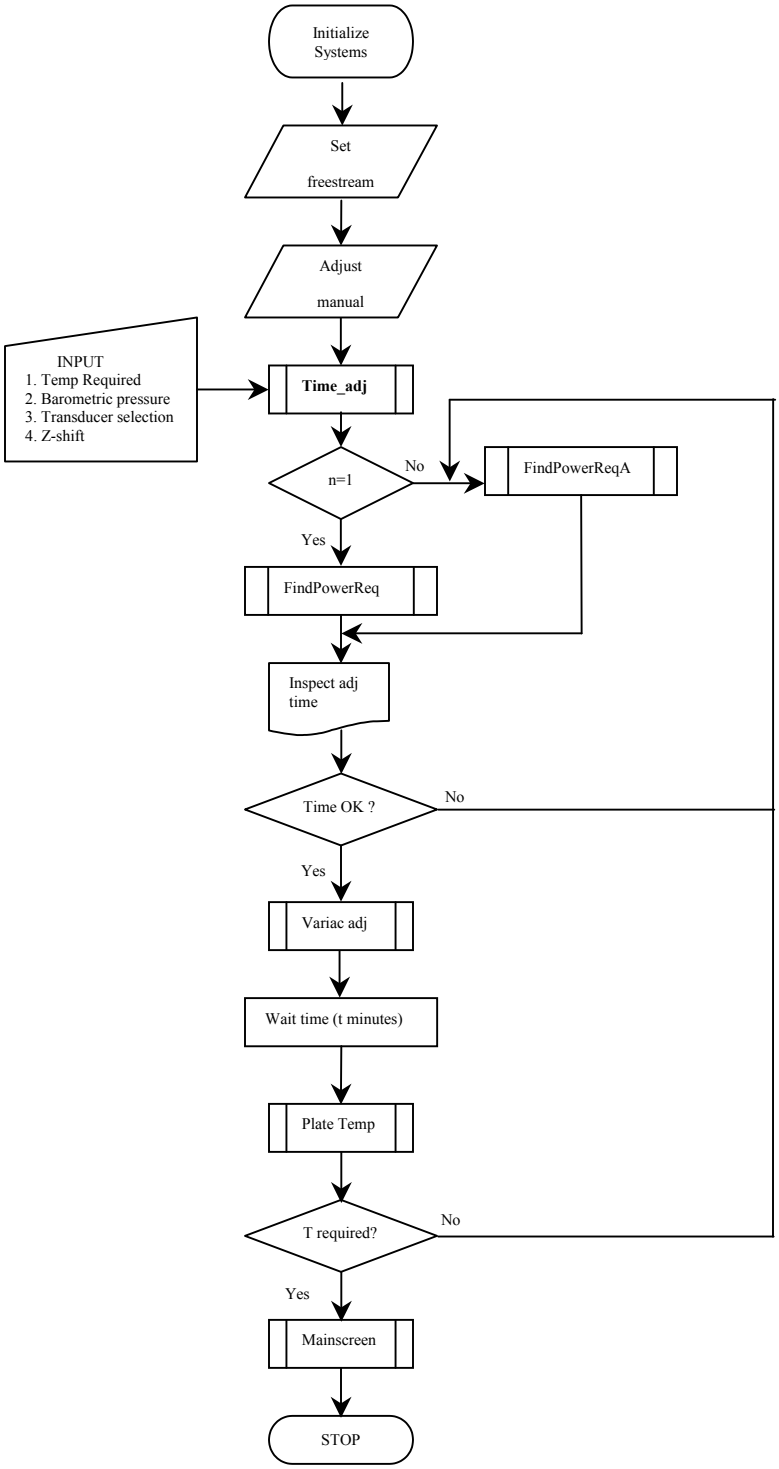

Figure B.1 Algorithm for the Control of The THTTF

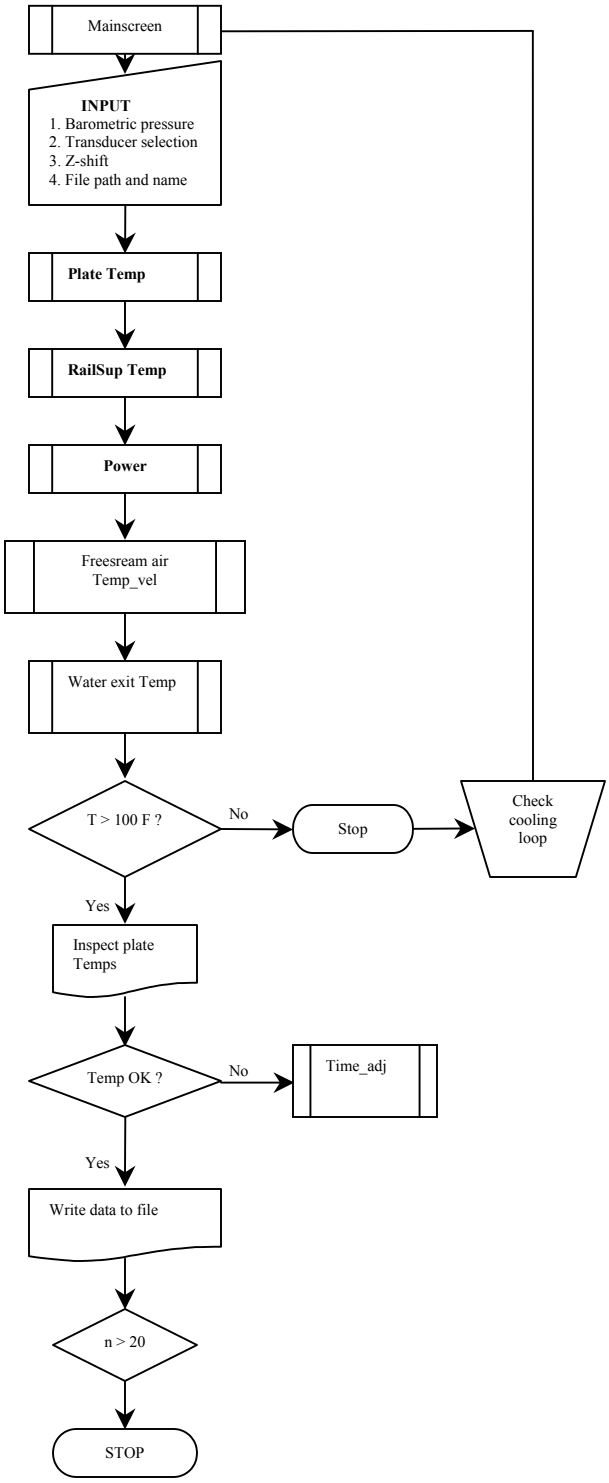

Figure B.2 Algorithm For Data Acquisition on the THTTF

Table B.1 Channel Directory for HP-3497A

Channel #	Description
0	Switch shunt resistor in or out of circuit
1-24	Adjustment of motorised variacs
25	Adjustment of motorised variac for calibration plate
26-49	Switch watt transducer into test plate circuits
50	Switch watt transducer into power calibration plate circuit
52	Dump valve open
53	Dump valve close
54	Variac adjustment direction control
100-147	Plate thermistors
150	Rail support thermistor for plate 1
151	Water exit temperature
152	Rail support thermistor for plate 24
153	Freestream air temperature
154	Switch shunt resistor in or out of circuit
157	Used to replace channel 143 (bad)
300	Pressure transducer voltage
301-317	Rail support thermistors (for plates 2 to 23)
320	Manual variac voltage Vset1 (variacs 1-8)
322	Manual variac voltage Vset2 (variacs 9-16)
324	Manual variac voltage Vset3 (variacs 17-24)

WTdate

Inputs	Outputs
None	Date

SubVIs	Caller VIs
None	Mainscreen

Description

This VI acquires the current date from the PC and records this date in a file as specified by the filename dialogue box.

Variac adj

Inputs	Outputs
Variac adjustment time (sec)	None
Variac direction	
Plate number	

SubVIs	Caller VIs
WT_Close Channel-Variac	
WT_AllClose Channel	

Description

This VI is used to manually adjust the Powerstat-15M21 motor driven variable transformers that control the power supplied to each plate. The input includes the adjustment time in seconds and the plate number for which the power is to be adjusted. The direction of the motor (lower or raise) is also selected according to the power requirement of the selected plate.

Vset

Inputs	Outputs
None	Voltage readings from the 3 Variac W-10 transformers

SubVIs	Caller VIs
None	Time_adj

Description

This VI acquires voltage readings from the three Variac W-10 variable transformers. T he values obtained are used in the evaluation of the Stanton number in the first loop when calculating the power requirements to maintain a desired isothermal test surface.

Dump Valve adj

Inputs	Outputs
Motor adjustment time	None
Motor direction	

SubVIs	Caller VIs
WT_Close Channel	
WT_AllClose Channel	

Description

This VI controls the operation of the dump valve and has two inputs. The motor adjustment time is the input in seconds that determines how long the motor operates the valve. The maximum adjustment time is limited to five seconds, which is the time required to close the valve completely from a fully open position or vice versa. The motor direction determines the action of the control to either open or close the valve.

AirSpeedControl

Inputs	Outputs
Input Voltage	None

SubVIs	Caller VIs
W_T3497A Dig Open_Close Channel	

Description

This VI is used to control the speed of the blower motor remotely from the ADACS. The input is a dc voltage signal with a range of 0 to +10 V generated by the HP-3497A. The blower speed increases with the voltage supplied. The air speed can be controlled via this VI.

FindPowerReq

Inputs	Outputs
Barometric pressure	Freestream velocity
Z-Shift	Freestream temperature
Temperature required	Power required
Pressure transducer selection	
Freestream velocity	
Freestream temperature	

SubVIs	Caller VIs
Free Stream airTemp_Vel	Time_adj

Description

This VI computes the power requirement for each plate in order to maintain the desired set temperature. It uses the freestream velocity and temperature output from the sub VI "Free Stream airTemp_Vel" as one of its inputs. The appropriate pressure transducer selection and its corresponding zero shift value are also required inputs for this VI. The power requirement computation is used as an initial estimate for the positioning of the variacs.

FindPowerReqA

Inputs	Outputs
Barometric pressure	Freestream velocity
Z-Shift	Freestream temperature
Temperature required	Power required
Pressure transducer selection	
Freestream velocity	
Freestream temperature	

SubVIs	Caller VIs
Free Stream airTemp_Vel	Time_adj

Description

This VI computes the power requirement for each plate in order to maintain the desired set temperature. It is used to fine tune the position of the variacs based on the last power and plate temperature readings. The required inputs are similar to those of "FindPowerReq" but in addition requires the last acquired data for power and plate temperature.

Time_adj

Inputs	Outputs
Temperature required	Variac adjustment time

SubVIs	Caller VIs
FindPowerReq	None
FindPowerReqA	
Power	
Plate Temp	
RailSup Temp	
Vset	
Variac adj	

Description

This is the main program that monitors and controls the THTTF. It is responsible for continuous measurement of plate temperature at timed intervals, and for computing the power required to attain the set point and adjusting the variacs appropriately. The first loop utilizes output from FindPowerReq to establish an initial setting for the variacs. Subsequent loops utilize the output from FindPowerReqA as a basis for computing the difference between the current condition and the required condition.

Mainscreen

Inputs	Outputs
Barometric pressure	Plate temperature
Z-Shift	Time elapsed
Pressure transducer selection	
File path/name	

SubVIs	Caller VIs
WT_3497A Initialize	None
Power	
Plate Temp	
RailSup Temp	
Free stream airTemp_Vel	
B_Ltemp	
Water exit Temp	

Description

This is the main data acquisition program that plots and displays the temperature history for each plate. Mainscreen has a write data option which allows the user to determine when data are to be recorded. With the write data option activated, the acquired data are written to a spreadsheet file as specified in the file path dialogue box. The following data are written for each cycle of mainscreen executed: elapsed time, freestream velocity, recovery temperature, plate temperatures, rail support temperatures, plate powers, exit water temperature, barometric

pressure, and air density. A spreadsheet program in MS Excel is used to manipulate the acquired data to evaluate the required quantities of interest: static temperature, Total temperature, conductive loss, radiation loss, x-Reynolds number, and Stanton number. The same MS Excel workbook is used to plot the reported charts of Stanton number vs. x-Reynolds number.

PlateTemp

Inputs	Outputs
First channel	Plate temperatures
Last channel	

SubVIs	Caller VIs
W_T 3497A Analog Scan & Read	None

Description

This VI sequentially scans the HP 3497A from the first channel specified to the last channel specified. The first channel is 100 and corresponds to the left thermistor mounted on plate 1 while the second channel (101) represents the right thermistor mounted on plate 1. The Plate Temp VI measures the resistance of each of the thermistors and converts it into a temperature reading using the Steinhart-Hart equation.

RailSupTemp

Inputs	Outputs
First channel	Rail temperatures
Last channel	
File path/name	

SubVIs	Caller VIs
W_T 3497A Analog Scan & Read Rail	None

Description

This VI sequentially scans the HP 3497A from the first channel specified to the last channel specified and plots the temperature history of the support rails. The VI measures the resistance of each of the thermistors and converts the resistance reading into a temperature reading using the Steinhart-Hart equation.

Free stream airTemp_Vel

Inputs	Outputs
Barometric pressure	Freestream velocity
Z-shift	Recovery temperature
Pressure transducer selection	Air density

SubVIs	Caller VIs
WT_Close Channel	Mainscreen
WTvoltmeter	
WTvoltmeter_P	
WT_velocity	

Description

This VI measures and displays the freestream velocity and the freestream recovery temperature and calculates the density of the air.

Water exitTemp

Inputs	Outputs
None	Water exit temperature

SubVIs	Caller VIs
WT_Close Channel	Mainscreen
WTvoltmeter	
WaterTempWarning	

Description

This VI measures and displays the resistance of the thermistor used for measurement of the temperature of the water in the cooling system.

WaterTempWarning

Inputs	Outputs
Water exit temperature	None

SubVIs	Caller VIs
Beep	Water exitTemp

Description

This VI monitors the temperature of the water in the cooling system and ensures that the air is adequately cooled. This is a protective function that sounds the alarm beeper, displays a warning message, and aborts the program when the exit water temperature exceeds 100^{o}F.

power

Inputs	Outputs
First channel	Power array
Last channel	

SubVIs	Caller VIs
3497A Power Analog Scan Configure	Mainscreen
WTvoltmeter_Q	
WT_3497A Voltmeter Trigger	
3497A Analog Step	
W_T 3497A Power Analog Scan & Read	

Description

This VI scans the HP 3497A from the first channel to the last channel specified. Because the HP 3456A voltmeter cannot measure current directly, this VI indirectly measures the current output of the Watt transducer by taking a voltage reading across the shunt resistor and the resistance of the shunt resistor. The power calculated in Watt is plotted and displayed for the 24 plates.

DPWarning

Inputs	Outputs
Differential pressure	None

SubVIs	Caller VIs
Beep	WT_velocity

Description

This VI monitors the differential pressure at the Validyne transducers in order to ensure that the range of the transducer is not exceeded. This is a protective function that sounds the alarm beeper, displays a warning message, and aborts the program when the output voltage of the transducer exceeds 5 volts. This prompts the user to change to the higher range transducer or troubleshoot for any problems.

WT_validyne pressure difference

Inputs	Outputs
Transducer selection	Output voltage
Z-shift	Pressure differential

SubVIs	Caller VIs
DPWarning	WT_velocity
Beep	Mainscreen
Mean	
WTvoltmeter_P	
WT_Close Channel	

Description

This VI measures the dc voltage output from the selected pressure transducer and converts it to a differential pressure reading using the appropriate calibration equation for that transducer. The VI directs the HP 3456A to take 10 readings, each with one power line integration time. These 10 readings are and then averaged together. Both transducers exhibited a small but stable voltage output at zero pressure. This zero shift (Z-shift) is corrected for by subtracting it from the measured voltage.

WT_velocity

Inputs	Outputs
Barometric pressure	Freestream velocity
Z-shift	Air density
Transducer selection	
Recovery temperature	

SubVIs	Caller VIs
WT_Close Channel	Free stream airTemp_Vel
WTvoltmeter_P	Mainscreen
DPWarning	
WT_validyne pressure difference	

Description

This VI measures and displays the freestream velocity and calculates the density of the air.

The following sub VIs are modified from the standard drivers provided by National Instruments for the control of the respective HP equipment.

1. Plate Analog Scan & Read.vi
2. W_T 3497A Analog Scan & Read.vi
3. W_T 3497A Power Analog Scan & Read.vi
4. W_T 3497A Dig Open_close Channel.vi
5. WT_3497A Initialize.vi
6. WT_ 3497A Voltmeter Trigger.vi
7. WT_ AllClose Channel.vi
8. WT_ChannelAdvance.vi
9. WT_ Close Channel.vi
10. WT_ Close Channel_R.vi
11. WT_ Close Channel_Q.vi
12. WT_ Close Channel-Variac.vi
13. WT_ RelayClose Channel.vi
14. WTvoltmeter.vi
15. WTvoltmeter_P.vi
16. WTvoltmeter_Q.vi
17. WTvoltmeter_Q_R.vi
18. WTvoltmeter_Q_V.vi
19. WTvoltmeter_T.vi
20. WTvoltmeter_Vset.vi

APPENDIX C

TABULATION OF EXPERIMENTAL DATA

Table C.1 Heat Transfer Data at Freestream Velocity of 27.8 m/s taken on 07/02/02

U_{inf} = 27.8 m/s	T_r = 27.6 °C	Cp = 1010 J/kg-C	Date : 07/02/02
P_{bar} = 30.14 in_Hg	T_{inf} = 27.3 °C	Rho = 1.1693 kg/m^3	
Mu = 1.86E-05 kg/m-s	T_0 = 27.7 °C	U_{eff} = 0.42 W/K	

PLATE #	x (m)	T_P (°C)	T_{rail} (°C)	P (W)	Q_c (W)	Q_r (W)	Re_x	St
1	0.05	44.1	45.4	105.1	-0.57	0.57	8.855E+04	0.00414
2	0.15	44.2	46.5	69.6	-0.95	0.58	2.656E+05	0.00273
3	0.25	44.1	45.2	60.6	-0.49	0.57	4.427E+05	0.00238
4	0.36	44.2	45.7	56.8	-0.64	0.58	6.375E+05	0.00222
5	0.46	44.2	45.9	53.8	-0.70	0.58	8.146E+05	0.00210
6	0.56	44.3	46.1	51.8	-0.77	0.58	9.917E+05	0.00202
7	0.66	44.4	46.2	49.8	-0.77	0.59	1.169E+06	0.00193
8	0.76	44.2	46.2	48.4	-0.84	0.58	1.346E+06	0.00190
9	0.86	44.3	46.6	46.6	-0.94	0.58	1.523E+06	0.00182
10	0.97	44.3	46.9	45.1	-1.10	0.58	1.718E+06	0.00177
11	1.07	44.2	46.3	44.7	-0.87	0.58	1.895E+06	0.00176
12	1.17	44.3	45.6	44.7	-0.57	0.58	2.072E+06	0.00174
13	1.27	44.4	45.9	44.1	-0.63	0.59	2.249E+06	0.00170
14	1.37	44.3	46.1	43.1	-0.76	0.58	2.426E+06	0.00168
15	1.47	44.4	46.2	44.0	-0.76	0.59	2.603E+06	0.00171
16	1.58	44.4	46.2	43.4	-0.75	0.59	2.798E+06	0.00168
17	1.68	44.5	46.4	43.8	-0.83	0.59	2.975E+06	0.00169
18	1.78	44.2	46.7	40.8	-1.05	0.58	3.152E+06	0.00161
19	1.88	44.4	46.5	40.7	-0.87	0.59	3.329E+06	0.00158
20	1.98	44.4	46.3	41.2	-0.81	0.59	3.506E+06	0.00160
21	2.08	44.3	45.3	40.9	-0.42	0.58	3.683E+06	0.00158
22	2.18	44.1	44.3	40.3	-0.09	0.58	3.861E+06	0.00157
23	2.29	44.2	43.7	41.2	0.22	0.58	4.055E+06	0.00157
24	2.39	44.2	42.1	49.5	0.87	0.58	4.232E+06	0.00188

Table C.2 Heat Transfer Data at Freestream Velocity of 42.9 m/s taken on 06/26/02

U_{inf} = 42.86 m/s	T_r = 30.0 °C	Cp = 1010 J/kg-C	Date: 06/26/02
P_{bar} = 30.11 in_Hg	T_{inf} = 29.2 °C	Rho = 1.693 kg/m^3	
Mu = 1.86E-05 kg/m-s	T_0 = 30.1 °C	U_{eff} = 0.42 W/K	

PLATE #	x (m)	T_P (°C)	T_{rail} (°C)	P (W)	Q_c (W)	Q_r (W)	Re_x	St
1	0.05	44.5	45.8	120.3	-0.55	0.53	1.347E+05	0.00355
2	0.15	44.7	47.7	82.3	-1.25	0.54	4.042E+05	0.00241
3	0.25	44.9	46.8	74.6	-0.79	0.55	6.736E+05	0.00215
4	0.36	44.8	47.6	67.6	-1.19	0.54	9.700E+05	0.00198
5	0.46	44.5	47.8	61.4	-1.40	0.53	1.239E+06	0.00183
6	0.56	44.7	48.1	61.6	-1.43	0.54	1.509E+06	0.00182
7	0.66	44.6	48.1	58.4	-1.47	0.53	1.778E+06	0.00173
8	0.76	44.8	48.1	58.6	-1.40	0.54	2.048E+06	0.00172
9	0.86	44.7	48.2	55.9	-1.50	0.54	2.317E+06	0.00166
10	0.97	44.6	48.3	53.9	-1.58	0.53	2.614E+06	0.00161
11	1.07	44.8	47.6	54.6	-1.20	0.54	2.883E+06	0.00160
12	1.17	44.9	46.9	55.1	-0.85	0.54	3.152E+06	0.00159
13	1.27	44.8	47.3	53.1	-1.04	0.54	3.422E+06	0.00155
14	1.37	44.9	47.7	52.8	-1.20	0.54	3.691E+06	0.00153
15	1.47	44.7	47.8	52.1	-1.33	0.54	3.961E+06	0.00154
16	1.58	44.7	47.9	50.3	-1.36	0.54	4.257E+06	0.00149
17	1.68	44.9	48.2	51.1	-1.42	0.54	4.526E+06	0.00150
18	1.78	44.8	48.6	49.4	-1.56	0.54	4.796E+06	0.00145
19	1.88	44.8	48.3	50.5	-1.45	0.54	5.065E+06	0.00148
20	1.98	44.7	48.0	51.9	-1.38	0.54	5.335E+06	0.00153
21	2.08	44.6	47.1	48.7	-1.06	0.53	5.604E+06	0.00144
22	2.18	44.6	46.2	50.0	-0.66	0.53	5.874E+06	0.00147
23	2.29	44.7	45.6	49.8	-0.36	0.54	6.170E+06	0.00144
24	2.39	44.7	43.8	51.4	0.39	0.54	6.439E+06	0.00147

Table C.3 Heat Transfer Data at Freestream Velocity of 43.2 m/s taken on 05/17/02

U_{inf} = 43.2 m/s T_r = 31.9 °C Cp = 1010 J/kg-C Date: 05/17/02

P_{bar} = 29.8 in_Hg T_{inf} = 31.1 °C Rho = 1.1533 kg/m^3

Mu = 1.86E-05 kg/m-s T_0 = 32.0 °C U_{eff} = 0.42 W/K

PLATE #	x (m)	T_P (°C)	T_{rail} (°C)	P (W)	Q_c (W)	Q_r (W)	Re_x	St
1	0.05	45.9	45.7	120.8	0.073	0.52	1.339E+05	0.00369
2	0.15	45.9	47.9	78.2	-0.838	0.52	4.017E+05	0.00242
3	0.25	45.9	47.4	69.0	-0.649	0.52	6.695E+05	0.00213
4	0.36	45.9	48.4	64.0	-1.069	0.52	9.641E+05	0.00199
5	0.46	45.9	48.6	59.8	-1.124	0.52	1.232E+06	0.00185
6	0.56	45.9	48.8	58.2	-1.225	0.52	1.500E+06	0.00181
7	0.66	46.0	49.0	57.1	-1.251	0.53	1.768E+06	0.00176
8	0.76	45.8	49.2	54.9	-1.396	0.52	2.035E+06	0.00172
9	0.86	45.9	48.8	53.5	-1.214	0.52	2.303E+06	0.00167
10	0.97	45.8	48.4	51.6	-1.084	0.52	2.598E+06	0.00161
11	1.07	45.9	47.6	52.2	-0.695	0.52	2.866E+06	0.00160
12	1.17	46.0	46.8	52.7	-0.322	0.53	3.133E+06	0.00160
13	1.27	46.0	47.6	51.8	-0.677	0.53	3.401E+06	0.00158
14	1.37	46.0	48.5	50.3	-1.031	0.53	3.669E+06	0.00155
15	1.47	45.9	48.7	50.0	-1.198	0.52	3.937E+06	0.00156
16	1.58	45.9	49.0	47.7	-1.305	0.52	4.231E+06	0.00150
17	1.68	46.0	49.0	48.9	-1.292	0.52	4.499E+06	0.00152
18	1.78	45.9	49.1	47.1	-1.368	0.52	4.767E+06	0.00148
19	1.88	45.9	49.2	47.7	-1.356	0.52	5.035E+06	0.00149
20	1.98	45.9	49.2	49.3	-1.371	0.52	5.303E+06	0.00154
21	2.08	45.9	47.8	46.8	-0.783	0.52	5.570E+06	0.00144
22	2.18	45.9	47.1	47.5	-0.507	0.52	5.838E+06	0.00146
23	2.29	46.0	45.5	47.5	0.213	0.52	6.133E+06	0.00143
24	2.39	45.9	43.4	48.8	1.036	0.52	6.401E+06	0.00146

Table C.4 Heat Transfer Data at Freestream Velocity of 42.8 m/s taken on 07/10/02

U_{inf} = 42.8 m/s	T_r = 30.2 °C	Cp = 1010 J/kg-C	Date: 07/02/02
P_{bar} = 30.0 in_Hg	T_{inf} = 29.4 °C	Rho = 1.1693 kg/m^3	
Mu = 1.86E-05 kg/m-s	T_0 = 30.3 °C	U_{eff} = 0.42 W/K	

PLATE #	x (m)	T_P (°C)	T_{rail} (°C)	P (W)	Q_c (W)	Q_r (W)	Re_x	St
1	0.05	45.4	49.1	126.0	-1.57	0.56	1.345E+05	0.00358
2	0.15	45.7	51.1	84.7	-2.28	0.57	4.034E+05	0.00239
3	0.25	45.9	50.4	77.7	-1.87	0.58	6.723E+05	0.00215
4	0.36	45.7	51.4	70.4	-2.36	0.57	9.681E+05	0.00199
5	0.46	45.5	51.5	64.0	-2.54	0.56	1.237E+06	0.00185
6	0.56	45.6	51.7	64.2	-2.54	0.56	1.506E+06	0.00184
7	0.66	45.5	51.6	61.2	-2.56	0.56	1.775E+06	0.00177
8	0.76	45.9	51.5	61.3	-2.36	0.57	2.044E+06	0.00172
9	0.86	45.9	51.5	60.0	-2.33	0.58	2.313E+06	0.00168
10	0.97	45.8	51.5	57.8	-2.38	0.57	2.609E+06	0.00164
11	1.07	45.2	50.6	54.7	-2.31	0.55	2.877E+06	0.00162
12	1.17	45.6	49.8	57.0	-1.77	0.57	3.146E+06	0.00161
13	1.27	45.7	50.3	55.0	-1.93	0.57	3.415E+06	0.00156
14	1.37	45.8	50.8	54.0	-2.09	0.57	3.684E+06	0.00152
15	1.47	45.9	50.9	56.0	-2.11	0.58	3.953E+06	0.00157
16	1.58	46.0	51.1	53.9	-2.14	0.58	4.249E+06	0.00150
17	1.68	46.0	51.4	53.7	-2.27	0.58	4.518E+06	0.00150
18	1.78	45.7	51.7	50.4	-2.52	0.57	4.787E+06	0.00144
19	1.88	45.9	51.5	52.9	-2.35	0.58	5.056E+06	0.00149
20	1.98	45.9	51.2	54.5	-2.25	0.57	5.325E+06	0.00154
21	2.08	45.7	50.1	51.5	-1.83	0.57	5.594E+06	0.00145
22	2.18	45.7	49.0	52.3	-1.39	0.57	5.862E+06	0.00147
23	2.29	45.8	48.2	52.5	-1.02	0.57	6.158E+06	0.00145
24	2.39	45.8	46.1	53.9	-0.11	0.57	6.427E+06	0.00147

Table C.5 Heat Transfer Data at Freestream Velocity of 60.9 m/s taken on 07/01/02

U_{inf} = 60.9 m/s T_r = 32.3 °C Cp = 1010 J/kg-C Date: 07/01/02

P_{bar} = 30.1 in_Hg T_{inf} = 30.7 °C Rho = 1.1693 kg/m^3

Mu = 1.86E-05 kg/m-s T_0 = 32.6 °C U_{eff} = 0.42 W/K

PLATE #	x (m)	T_P (°C)	T_{rail} (°C)	P (W)	Q_c (W)	Q_r (W)	Re_x	St
1	0.05	44.2	49.8	127.0	-2.35	0.47	1.913E+05	0.00329
2	0.15	44.4	51.6	85.8	-3.01	0.48	5.739E+05	0.00223
3	0.25	44.6	50.8	78.4	-2.60	0.48	9.564E+05	0.00200
4	0.36	44.5	51.5	71.2	-2.97	0.48	1.377E+06	0.00185
5	0.46	44.2	51.6	64.7	-3.08	0.47	1.760E+06	0.00172
6	0.56	44.3	51.6	64.7	-3.05	0.48	2.142E+06	0.00170
7	0.66	44.1	51.4	61.7	-3.09	0.46	2.525E+06	0.00167
8	0.76	44.2	51.2	61.8	-2.93	0.47	2.908E+06	0.00164
9	0.86	44.4	51.2	60.7	-2.86	0.48	3.290E+06	0.00159
10	0.97	44.4	51.3	58.4	-2.89	0.48	3.711E+06	0.00153
11	1.07	44.3	50.6	56.9	-2.65	0.47	4.094E+06	0.00151
12	1.17	44.4	49.9	57.6	-2.33	0.48	4.476E+06	0.00150
13	1.27	44.4	50.2	55.7	-2.44	0.48	4.859E+06	0.00145
14	1.37	44.4	50.5	54.6	-2.55	0.48	5.241E+06	0.00142
15	1.47	44.5	50.6	56.7	-2.56	0.48	5.624E+06	0.00147
16	1.58	44.6	50.7	54.6	-2.58	0.48	6.045E+06	0.00141
17	1.68	44.6	51.0	54.3	-2.68	0.48	6.427E+06	0.00140
18	1.78	44.4	51.2	52.8	-2.88	0.48	6.810E+06	0.00140
19	1.88	44.4	51.0	53.7	-2.79	0.48	7.192E+06	0.00142
20	1.98	44.2	50.8	53.9	-2.76	0.47	7.575E+06	0.00143
21	2.08	44.2	49.8	54.4	-2.34	0.47	7.958E+06	0.00144
22	2.18	44.1	48.7	52.9	-1.93	0.46	8.340E+06	0.00141
23	2.29	44.1	47.9	53.1	-1.58	0.47	8.761E+06	0.00140
24	2.39	44.5	46.0	65.0	-0.63	0.48	9.144E+06	0.00163